Supporting information for

One-Pot, Room-Temperature Conversion of CO_2 into Porous Metal−Organic Frameworks

Kentaro Kadota[†], You-lee Hong[⊥,§], Yusuke Nishiyama[⊥,#], Easan Sivaniah[†,§], Daniel Packwood[§], and Satoshi Horike*[‡,§,∥,¶]

[†]Department of Molecular Engineering, Graduate School of Engineering, and [‡]Department of Synthetic Chemistry and Biological Chemistry, Graduate School of Engineering, Kyoto University, Katsura, Nishikyo-ku, Kyoto 615-8510, Japan
[⊥]NMR Science and Development Division, RIKEN SPring-8 Center and RIKEN-JEOL Collaboration Center, Yokohama, Kanagawa 230-0045, Japan
[#]JEOL RESONANCE Inc., Musashino, Akishima, Tokyo 196-8558, Japan
[§]Institute for Integrated Cell-Material Sciences, Institute for Advanced Study, Kyoto University, Yoshida-Honmachi, Sakyo-ku, Kyoto 606-8501, Japan
[∥]AIST-Kyoto University Chemical Energy Materials Open Innovation Laboratory (ChEM-OIL), National Institute of Advanced Industrial Science and Technology (AIST), Yoshida-Honmachi, Sakyo-ku, Kyoto 606-8501, Japan
[¶]Department of Materials Science and Engineering, School of Molecular Science and Engineering, Vidyasirimedhi Institute of Science and Technology, Rayong 21210, Thailand

Table of Contents

Materials and general methods

All chemicals and solvents used in the syntheses were of reagent grade and used without any further purification. Zinc oxide (ZnO) nanopowder < 100 nm particle size, dimethylammonium dimethylcarbamate ($[NH_2Me_2][O_2CNMe_2]$), and 1,8-Diazabicyclo[5.4.0]undec-7-ene (DBU) were purchased from Sigma-Aldrich. Piperazine anhydrous (H_2PZ) >98%, (*S*)-(+)-2-methylpiperazine >97%, (*R*)-(−)-2-methylpiperazine >98%, *trans*-2,5-dimethylpiperazine >99%, and *cis*-2,6-dimethylpiperazine were purchased from Tokyo Chemical Industry Co., Ltd. Super dehydrated acetonitrile (MeCN), deoxidized tetrahydrofuran (THF), super dehydrated toluene, deoxidized methanol (MeOH), super dehydrated isopropanol (^{i}PrOH), and super dehydrated *N*,*N*-dimethylformamide (DMF) were purchased from Wako Pure Chemical Industries, Ltd. Zinc acetate dihydrate ($Zn(OAc)_2{\cdot}2H_2O$) from Nacalai Tesque, Inc.

Powder X-ray diffraction (PXRD): PXRD patterns were collected on a Rigaku MiniFlex with CuK_α anode. An air-sensitive sample holder was employed to collect PXRD pattern under Ar and the samples were sealed in the holder inside an Ar-filled glove box.

Synchrotron PXRD: Each powder sample was sealed in a Lindemann glass capillary inside an Ar-filled glove box. The synchrotron PXRD data were collected using synchrotron radiation (λ = 0.999000 Å) employing a large Debye-Scherrer camera with semiconductor detectors on the BL02B2 beamline at the Super Photon Ring (SPring-8, Hyogo, Japan). The first Bragg peak was fitted by the Lorenz function to calculate full-width half maximum (FWHM).

Rietveld refinement: The synchrotron PXRD data for the activated samples were utilized for the analysis. The initial structures for Rietveld refinement were constructed from the reported crystal structure of MOF-5 (CCDC code: SAHYIK). In the construction of the model structures for **2** and **3**, we assumed that the linker should have four different configurations resulted from the static disorder. As neither chiral solvents nor guest molecules were used, the configurations should be randomly observed, which leading to the formation of achiral MOF structures. The achiral space group, *Fm*-3*m* was employed sam as MOF-5. All the procedures were carried out using Rigaku PDXL2 software.

Single crystal X-ray diffraction (SC-XRD): SC-XRD experiments were performed with a Rigaku XtaLAB AFC10 diffractometer using a VariMax Mo Optic with Mo-Kα (λ = 0.71073 Å) The crystal structure was solved directly and refined by full-matrix

least-squares refinement using SHELXL 2017/1.

Fourier transform infrared (IR): IR spectra were collected using a Bruker Optics ALPHA FT-IR spectrometer with Universal ATR accessory under Ar.

Thermogravimetric analysis (TGA): TGA profiles were collected using a Rigaku Thermo plus TG 8121 apparatus in the temperature range of 40 to 500 °C at a heating rate of 10 °C min^{-1} under flowing Ar inside an Ar-filled glove box.

Gas adsorption: Gas adsorption isotherms were collected by a BELSORP-max (BEL Japan, Inc) equipped with a cryostat system. Brunauer–Emmett–Teller (BET) surface areas were calculated using N_2 adsorption isotherm data at 77 K. Each powder sample was activated at 80 °C under vacuum. A virial-type expression of the following form was used to fit the combined H_2 adsorption isotherm data at 77 and 87 K:

$$\ln P = \ln N + 1/T \sum_{i=0}^{m} a_i N_i + \sum_{i=0}^{n} b_i N_i$$

Here, P is the pressure expressed in Torr, N is the amount adsorbed in mmol/g, T is the temperature in K, a_i and b_i are virial coefficients, and m and n represent the number of coefficients required to adequately describe the isotherms. The equation was fit using the Origin software package. The values of the virial coefficients a_0 through a_m were then used to calculate the isosteric heat of adsorption using the following expression:

$$Q_{st} = -R \sum_{i=0}^{m} a_i Ni$$

Here, Q_{st} is the coverage-dependent isosteric heat of adsorption and R is the universal gas constant. The high-pressure CO_2 adsorption isotherm was collected by a BELSORP-HP (BEL Japan, Inc). The sample was activated at 80 °C under vacuum and packed under Ar.

Elemental analysis: CHN elemental analysis for the activated samples was quickly conducted under air on a MICRO CORDER JM11 (J-Science Lab Co., LTd.).

Scanning electron microscope (SEM): SEM images were captured using a Hitachi SU5000 instrument. The activated samples were quickly handled under air.

Solution nuclear magnetic resonance (NMR): ^{1}H NMR spectra were collected at 25 ºC on a Bruker Avance III instrument with AS500 magnet (500 MHz).

Solid-state magic angle spinning (MAS) nuclear magnetic resonance (NMR): All SSNMR spectra were performed at 14.1 T on a JNM-ECZ600R spectrometer with a 1 mm ^{1}H/X double-resonance MAS probe (JEOL RESONANCE Inc., Tokyo, Japan) under ambient temperature (~ 25 °C). 1D ^{13}C CP-MAS and 2D ^{1}H-^{13}C HETCOR SSNMR spectra were measured at MAS of 70 kHz and recycle delay of 11 sec. $\pi/2$ pulse lengths of ^{1}H and ^{13}C are 0.75 us and 1.15 us, respectively. The contact time of CP-MAS and HETCOR experiment was 4ms to observe the long range correlations between ^{1}H and ^{13}C nuclei.

X-ray absorption spectroscopy (XAS): X-ray absorption fine structure (XAFS) measurements XAS data were collected at the BL1.1W of the Synchrotron Light Research Institute (SLRI), Thailand. The spectra at the Zn K-edge (9659 eV) were measured in a fluorescence mode using a Si(111) double-crystal monochromator. Each sample was measured in powder form by placing the sample in a plastic frame sealed under Ar with polypropylene (PP) on the side and exposed to X-rays.

CO_2-temperature programmed desorption (TPD): TPD measurements were performed using MicrotracBEL BELCAT in the temperature range of 30−500 °C at a heating rate of 10 °C min^{-1} under Ar gas flow (30 mL min^{-1}). The sample (10 mg) was packed in the quartz-based measurement apparatus under Ar atmosphere.

Density functional theory (DFT) calculations: All-electron density functional theory (DFT) calculations were performed using the Fritz Haber Institute ab initio molecular simulations (FHI-aims) package version 171221_1[1]. Fragment structures were first relaxed using DFT with the PBE exchange-correlation functional[2] with Tkatchenko-Scheffler (TS) dispersion corrections[3], “light” basis set settings, and no spin-polarization. Starting the relaxed structures, structures with compressed and stretched Zn---O bonds were then prepared using an in-house script. Single-point energy calculations were then performed using the HSE06 exchange-correlation functional[4] with TS dispersion corrections[3], spin-polarization, and “tight” basis set settings. The HSE06 functional used 25 % Hartree-Fock exchange and range separation parameter 0.11 Bohr^{-1}. To explore how the choice of exchange-correlation approximation affects the results, the same calculations were also repeated using the LDA exchange correlation functional (Perdew-Wang 1992 parameterization)[5]. No significant qualitative differences were observed when using the LDA functional, indicating that our conclusions should be robust to exchange-correlation approximations.

Synthesis of $[Zn_4O(O_2CNMe_2)_6]$·toluene (Zn-SBU)[6-7].

A suspension of ZnO (1.00 g, 12.28 mmol) in dehydrated MeCN (100 mL) was mixed with $[NH_2Me_2][O_2CNMe_2]$ (20 mL, 156.5 mmol) in a 300 mL of round bottom flask inside an Ar-filled glovebox. The flask was sealed with a rubber septum and taken outside the glovebox. CO_2 gas (>99.99%) was flowed into the round bottom flask and the reaction mixture was stirred at 25 °C. After stirring overnight, the suspension turned into a colorless transparent solution, and the resulting solution was brought into the glovebox, filtrated, and the solvent was removed by evaporation at 25 °C. $[Zn(O_2CNMe_2)_2]$ was formed and dried under vacuum at 25 °C overnight (2.74 g, 92% yield). A suspension of $[Zn(O_2CNMe_2)_2]$ (2.41 g, 2.41 mmol) in dehydrated toluene (75 mL) was prepared in the glovebox. Deoxidized THF (15 mL) was quickly mixed with H_2O (44.9 μL) under air. The resulting THF/H_2O solution was added dropwise into the suspension of $[Zn(O_2CNMe_2)_2]$ under Ar flowing at 25 °C. The reaction mixture was stirred at 25 °C for 2 hours and heated up at 60 °C for 6 hours, the suspension turned into a colorless transparent solution. The resulting solution was filtrated and evaporated at 25 °C, and a white precipitate was formed and dried under vacuum at 25 °C (96% yield).

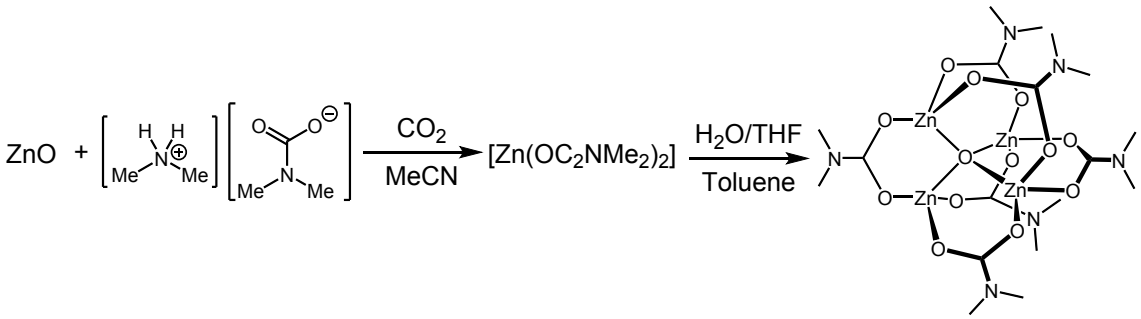

Synthesis of $[H_4PZ][PZ(CO_2)_2]$ ($PZ\text{-}CO_2$)[8].

A MeOH solution (5.0 mL) of H_2PZ (0.5 g, 5.80 mmol) was prepared in a 20 mL round bottom flask inside an Ar-filled glovebox. The flask was sealed with a rubber septum and taken outside the glovebox. CO_2 gas (>99.99%) was flowed into the round bottom flask at 25 °C. After 2 hours, colorless crystals were formed, and the flask was purged with Ar and taken inside the glovebox. The crystals were collected by filtration and washed with deoxidized MeOH under Ar, and dried under vacuum at 25 °C (15% yield).

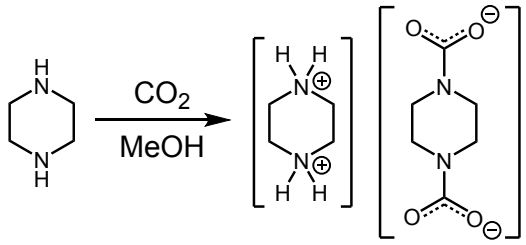

Synthesis of $[HDBU]_2[PZ(CO_2)_2]\cdot 2MeCN$ (PZ-CO_2-DBU).

To a MeCN solution (20 mL) of H_2PZ (344.6 mg, 4.00 mmol) in a 50 mL round bottom flask, DBU (1.196 mL, 8.00 mmol) was added dropwise inside an Ar-filled glovebox. The flask was sealed with a rubber septum and taken outside the glovebox. CO_2 gas (>99.99%) was flowed into the round bottom flask at 25 °C. After 12 hours, colorless crystals were formed, and the flask was purged with Ar and taken inside the glovebox. The crystals were collected by filtration and washed with anhydrous MeCN under Ar, and dried under vacuum at 25 °C (82% yield). The scale-up was possible up to 10 g of the product.

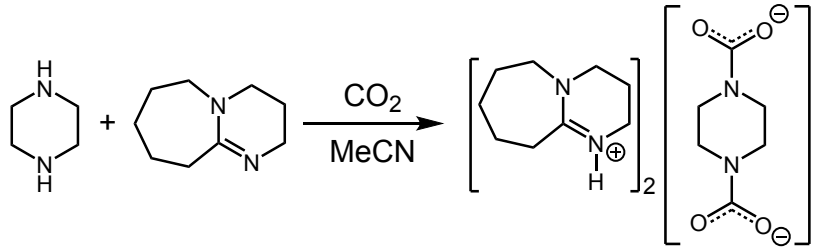

Synthesis of $[Zn_4O(PDC)_3]$ (1).

A 100 mL of DMF solution of $Zn(OAc)_2\cdot 2H_2O$ (878.0 mg, 4.00 mmol) was mixed with a 100 mL ^{i}PrOH solution of H_2PZ (258.4 mg, 3.00 mmol) and DBU (1.795 mL, 12.0 mmol) in a 300 mL round bottom flask at 25 °C inside an Ar-filled glovebox. The resultant transparent solution was stirred for 3 min. The flask was sealed with a rubber septum and taken outside the glovebox. CO_2 gas (>99.99%) was flowed into the round bottom flask at 25 °C. The white precipitate was formed immediately (< 10 sec). The reaction mixture was stirred under CO_2 flowing overnight to complete the reaction. The flask was purged with Ar and taken inside the glovebox. The precipitate was collected by filtration and washed with DMF and ^{i}PrOH under Ar, and dried under vacuum at 25 °C (80% yield, Calcd for $C_{18}H_{24}N_6O_{13}Zn_4$: C, 27.23; H, 3.05; N, 10.59. Found: C, 27.20; H, 4.17; N, 10.19.).

Method A. Synthesis of 1 from Zn-SBU and PZ-CO_2-DBU (1-A)

A 10 mL of ^{i}PrOH solution of **PZ-CO_2-DBU** (168.2 mg, 0.30 mmol) was added into a 10 mL of THF solution of **Zn-SBU** (90.4 mg, 0.10 mmol) under Ar at 25 °C. A white precipitate was formed immediately and kept at 25 °C overnight. The obtained precipitate was collected by filtration, and washed with ^{i}PrOH and THF under Ar, and dried under vacuum at 25 °C (94% yield).

Method B. Synthesis of 1 from $Zn(OAc)_2 \cdot 2H_2O$ and PZ-CO_2-DBU (1-B).

A 10 mL of ^{i}PrOH solution of **PZ-CO_2-DBU** (336.4 mg, 0.30 mmol) was added into a 10 mL of DMF solution of **Zn-SBU** (65.9 mg, 0.30 mmol) under Ar at 25 °C. A white precipitate was formed immediately and kept at 25 °C overnight. The obtained precipitate was collected by filtration, and washed with DMF and ^{i}PrOH under Ar, and dried under vacuum at 25 °C (85% yield).

Method C. Synthesis of 1 from $Zn(OAc)_2 \cdot 2H_2O$, H_2PZ and CO_2 without DBU (1-C)

The procedure of **1-C** was followed by that of **1** without using DBU (80% yield).

Synthesis of 1 using CO_2 from dried air (1-from-air).

The procedure of **1-from-air** was followed by that of **1** using compressed air gas (>99.99%) containing 400 ppm of CO_2 instead of pure CO_2 and reaction time was extended from overnight to 6 days (61% yield).

Synthetic attempt on 1 using NaOH (1-NaOH).

The procedure of **1-NaOH** was followed by that of **1** using NaOH instead of DBU.

Synthesis of $[Zn_4O(S\text{-mPDC})_3]$ (2, *S*-mPDC = (*S*)-(+)-2-methylpiperazine carbamate).

A 30 mL of DMF solution of $Zn(OAc)_2 \cdot 2H_2O$ (263.4 mg, 1.20 mmol) was mixed with a 30 mL ^{i}PrOH solution of (*S*)-(+)-2-methylpiperazine (90.2 mg, 0.90 mmol) and DBU (540 μL, 3.60 mmol) in a 100 mL round bottom flask at 25 °C inside an Ar-filled glovebox. The resultant transparent solution was stirred for 3 min. The flask was sealed with a rubber septum and taken outside the glovebox. CO_2 gas (>99.99%) was flowed into the round bottom flask at 25 °C. The white precipitate was formed immediately (<10 sec). The reaction mixture was stirred under CO_2 flowing overnight to complete the reaction. The flask was purged with Ar and taken inside the glovebox. The precipitate was collected by filtration and washed with DMF and ^{i}PrOH under Ar, and

dried under vacuum at 25 °C (80% yield, Calcd for $C_{21}H_{30}N_6O_{13}Zn_4$: C, 30.17; H, 3.62; N, 10.05. Found: C, 29.28; H, 4.45; N, 9.89.).

Large scale synthesis of 2 (2-large-scale).

A 1.5 L of DMF solution of $Zn(OAc)_2 \cdot 2H_2O$ (52.7 g, 2.4 mol) was mixed with a 1.5 L ^{i}PrOH solution of (*S*)-(+)-2-methylpiperazine (18.0 g, 1.8 mol) in a 5 L medium bottle at 25 °C under air. The resultant transparent solution was stirred for 5 min. The bottle was sealed with a rubber septum. CO_2 gas (>99.99%) was flowed into the round bottom flask at 25 °C. The white precipitate was formed (~15 min). The reaction mixture was stirred under CO_2 flowing for 3 days to complete the reaction. The precipitate was collected by filtration and washed with DMF and ^{i}PrOH under air, and dried under vacuum at 80 °C (ca. 50 g, 83% yield).

Synthesis of [Zn_4O(*R*-mPDC)$_3$] (3, *R*-mPDC = *R*-(−)-2-mehtylpiperazine carbamate).

The procedure of **3** was followed by that of **2** using (*R*)-(−)-2-methylpiperazine instead of (*S*)-(+)-2-methylpiperazine (84% yield, Calcd for $C_{21}H_{30}N_6O_{13}Zn_4$: C, 30.17; H, 3.62; N, 10.05. Found: C, 29.26; H, 4.08; N, 9.87.).

Synthesis of [Zn_4O(dmPDC)$_3$] (4, dmPDC = *trans*-2,5-dimethylpiperazine dicarbamate).

The procedure of **4** was followed by that of **2** using *trans*-2,5-dimethylpiperazine instead of (*S*)-(+)-2-methylpiperazine (59% yield, Calcd for $C_{24}H_{36}N_6O_{13}Zn_4$: C, 32.83; H, 4.13; N, 9.57. Found: C, 32.46; H, 4.66; N, 9.49.).

Table S1. List of carbamate-based coordination polymers[a]

No.	**CCDC code**	**Amines**	**Metal ions**
1	FIFROC	Propylamine	Cu^{+}
2	FUBCEM	Dimethylamine	Zn^{2+}
3	HYCOCD	Hydrazine	Cd^{2+}
4	HYCOMN	Hydrazine	Mn^{2+}
5	HYDCCD	Hydrazine	Cd^{2+}
6	HYZCZN	Hydrazine	Zn^{2+}
7	KEKWAZ	Hydrazine	Ni^{2+}, Li^{+}
8	KEKWED	Hydrazine	Co^{2+}, Li^{+}
9	MESNCB	Ammonia	Sn^{4+}
10	RABQOD	Dimethylamine	Bi^{3+}
11	SAFDOU	Dimethylamine	Zn^{2+}
12	SAQPUV	Dimethylamine	Ag^{+}
13	WEFJAS	Hydrazine	Ba^{2+}
14	WERFUV	Hydrazine	Na^{+}
15	XEZKEU	Hydrazine	Zn^{2+}
16	XEZKIY	Hydrazine	Co^{2+}
17	XISBIN	Pyrrole	Li^{+}

[a]Coordination polymers whose metal ions are linked by carbamate species are listed based on the CCDC 2019 using ConQuest as of December 6th, 2020.

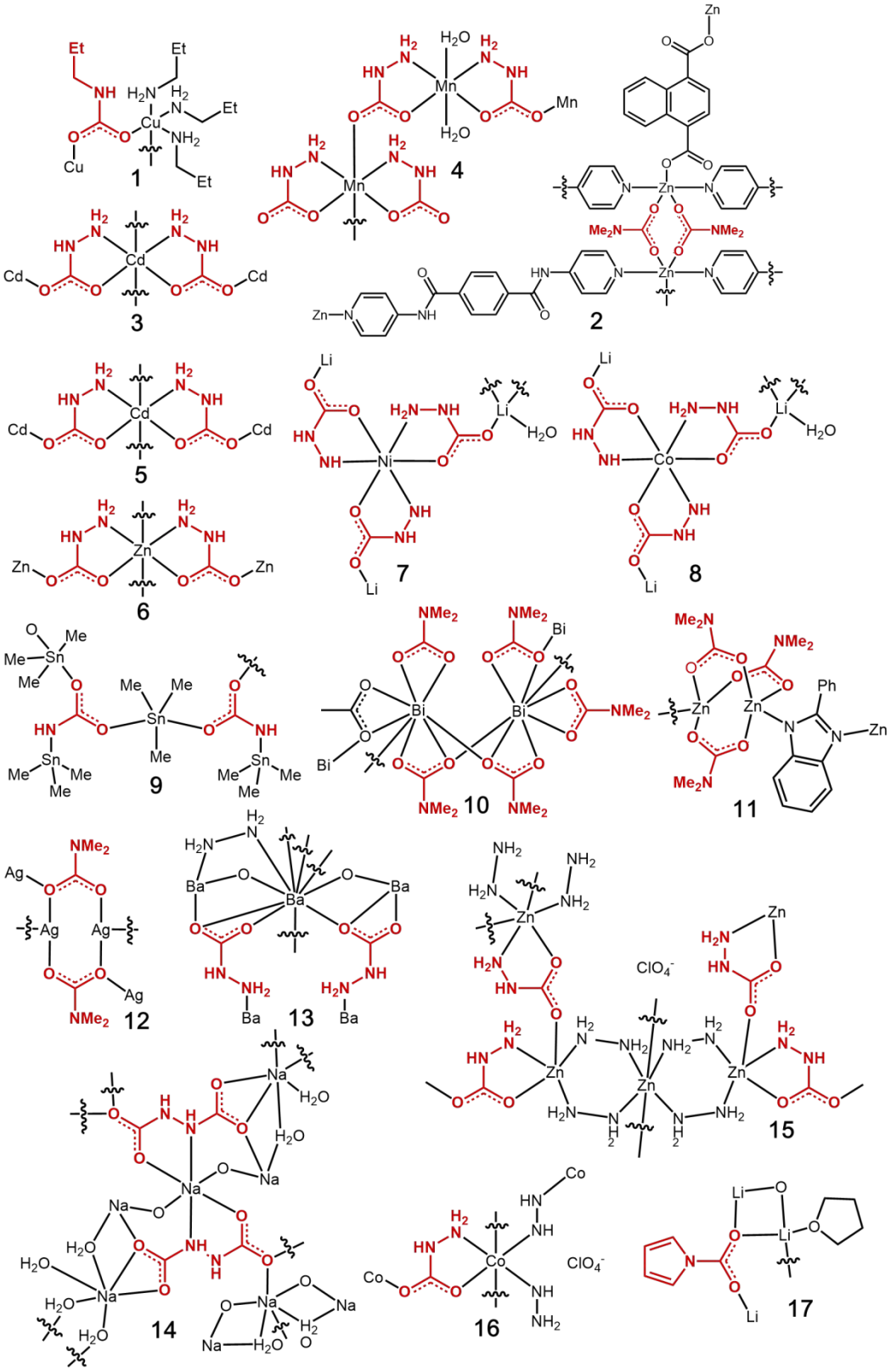

Figure S1. Structures of carbamate-based coordination polymers. The carbamate linkers are highlighted in red.

Figure S2. Image of the reaction system for the synthesis of **1**.

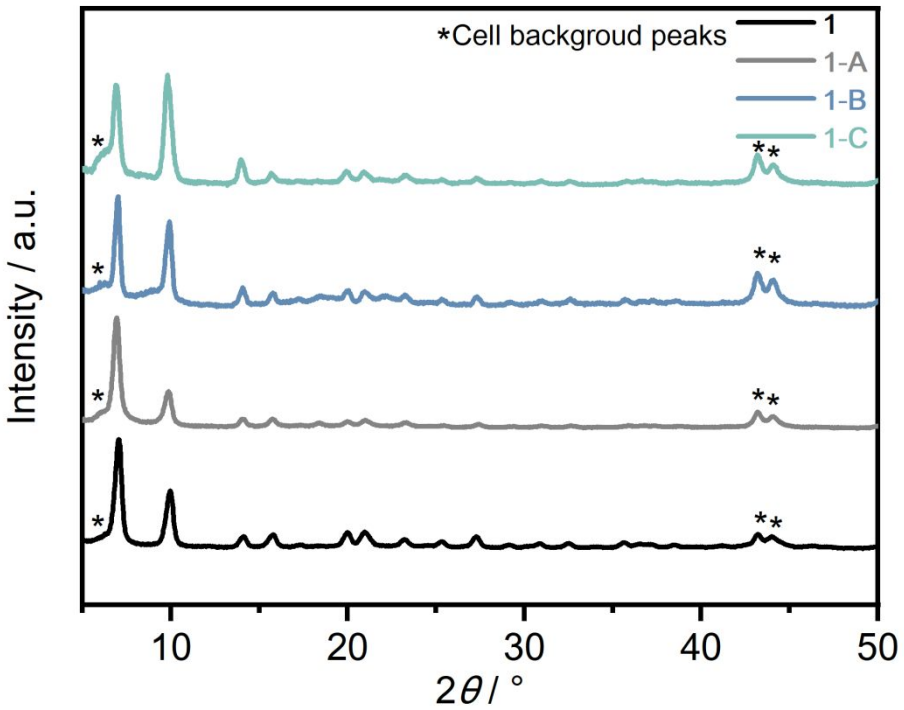

Figure S3. Lab-based PXRD patterns of as-synthesized **1**, **1-A**, **1-B**, and **1-C** under Ar.

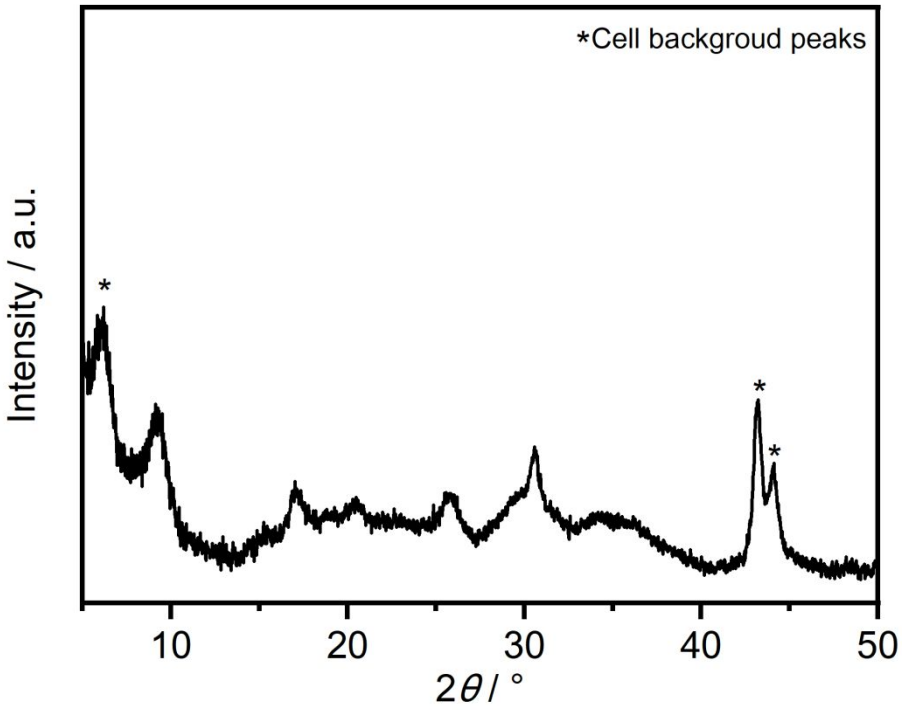

Figure S4. Lab-based PXRD pattern of as-synthesized **1-NaOH** under Ar.

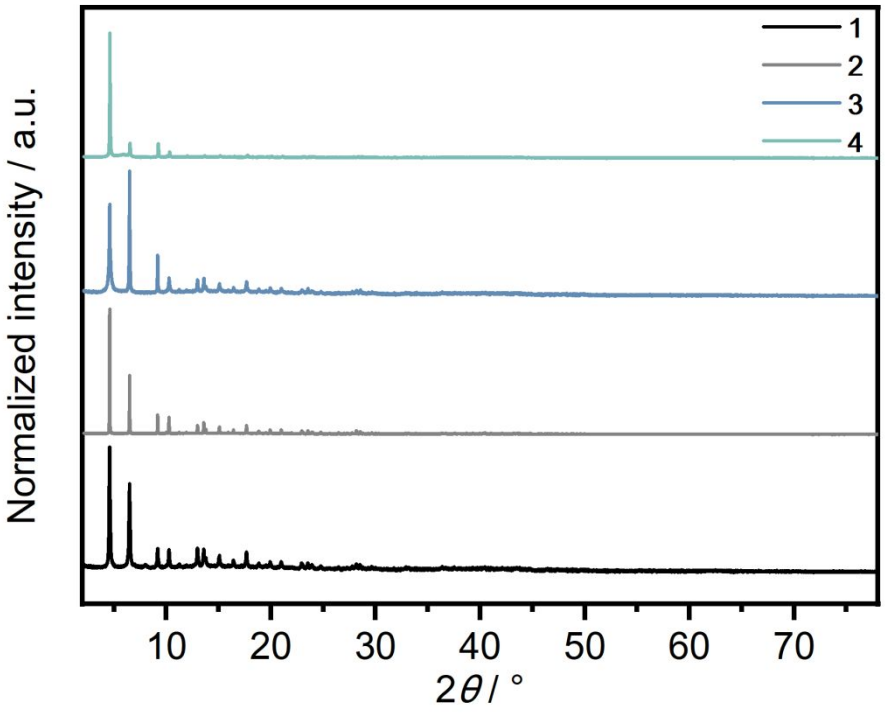

Figure S5. Synchrotron PXRD patterns of as-synthesized **1**−**4** under Ar.

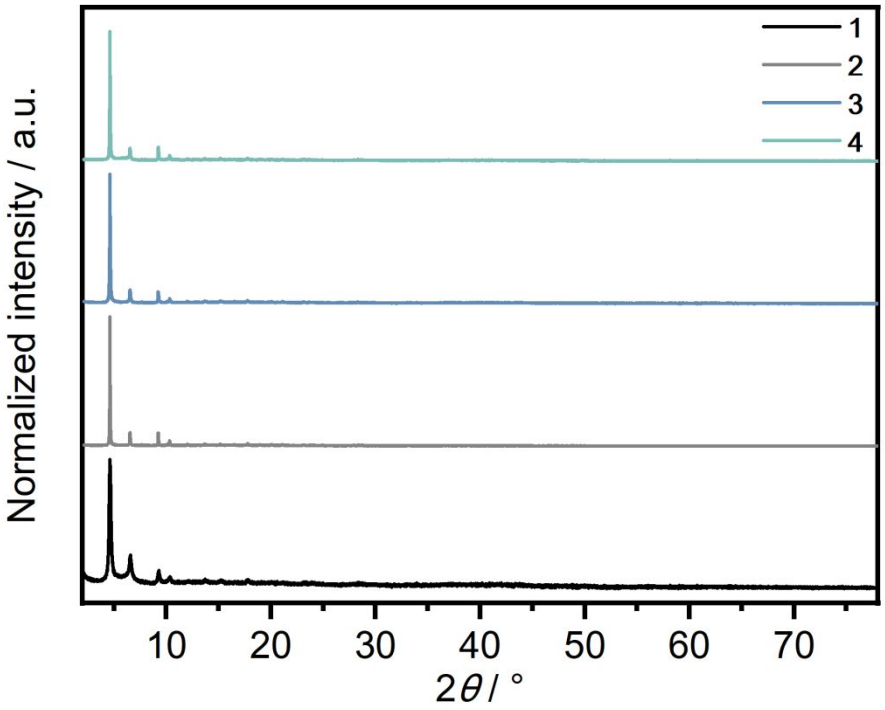

Figure S6. Synchrotron PXRD patterns of activated **1**−**4** under Ar.

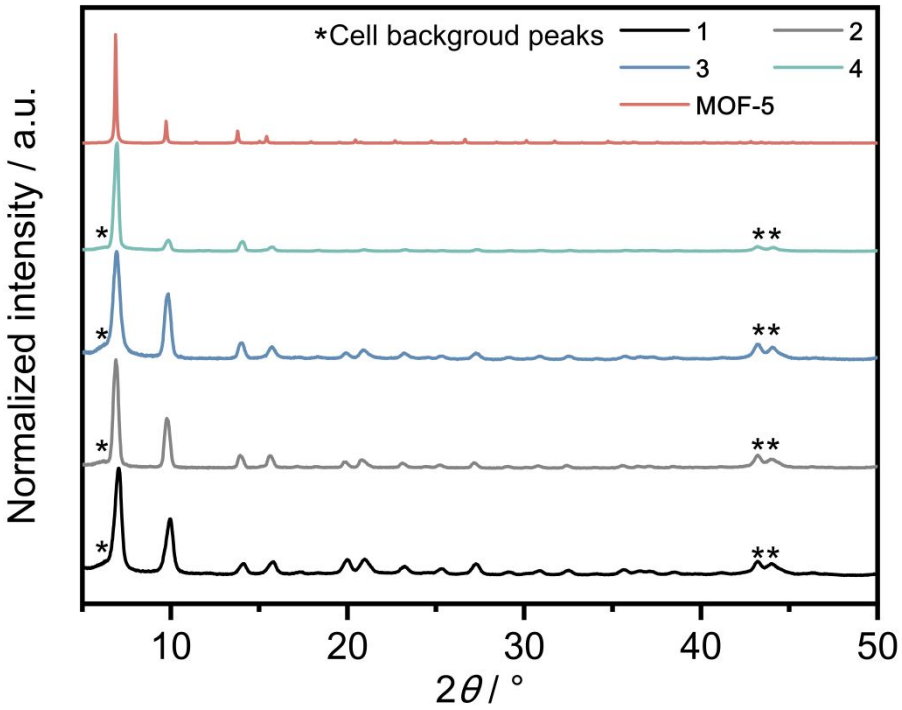

Figure S7. Lab-based PXRD patterns of as-synthesized **1**−**4** under Ar and simulated pattern of MOF-5.

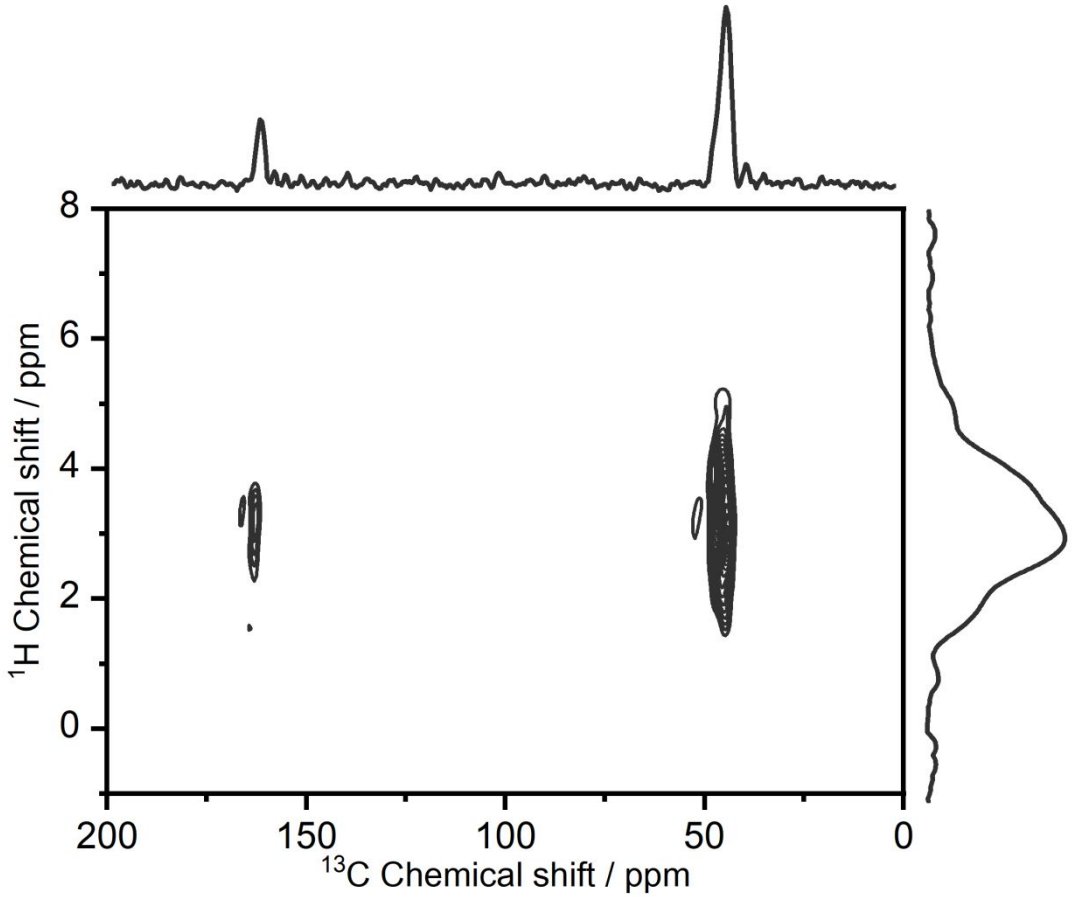

Figure S8. 2D ^{1}H-^{13}C HETCOR SSNMR spectrum of activated **1** under Ar.

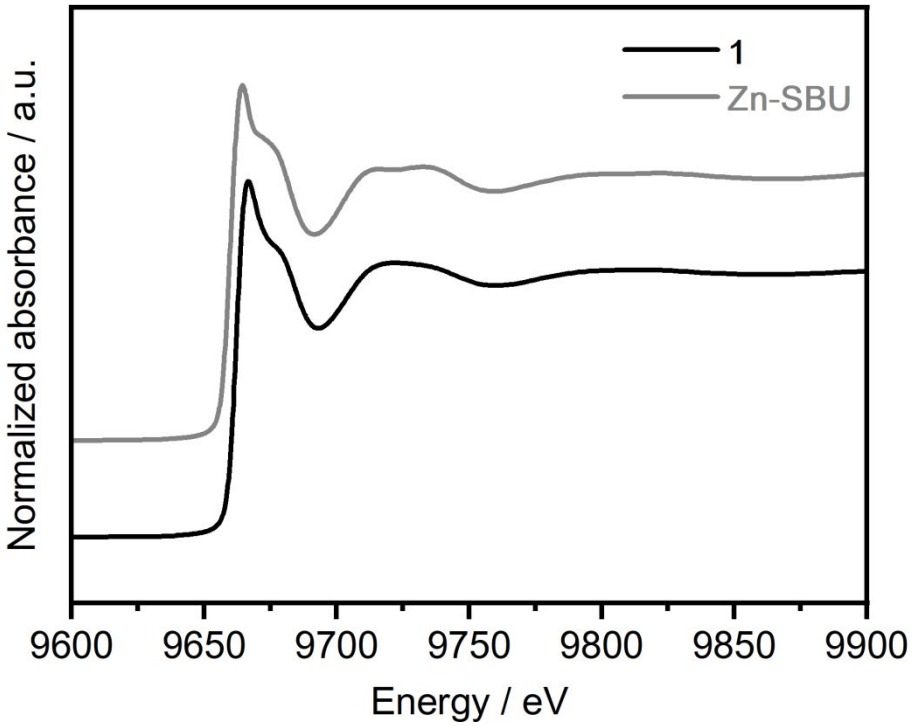

Figure S9. Zn K-edge XANES spectra of activated **1** and **Zn-SBU** under Ar.

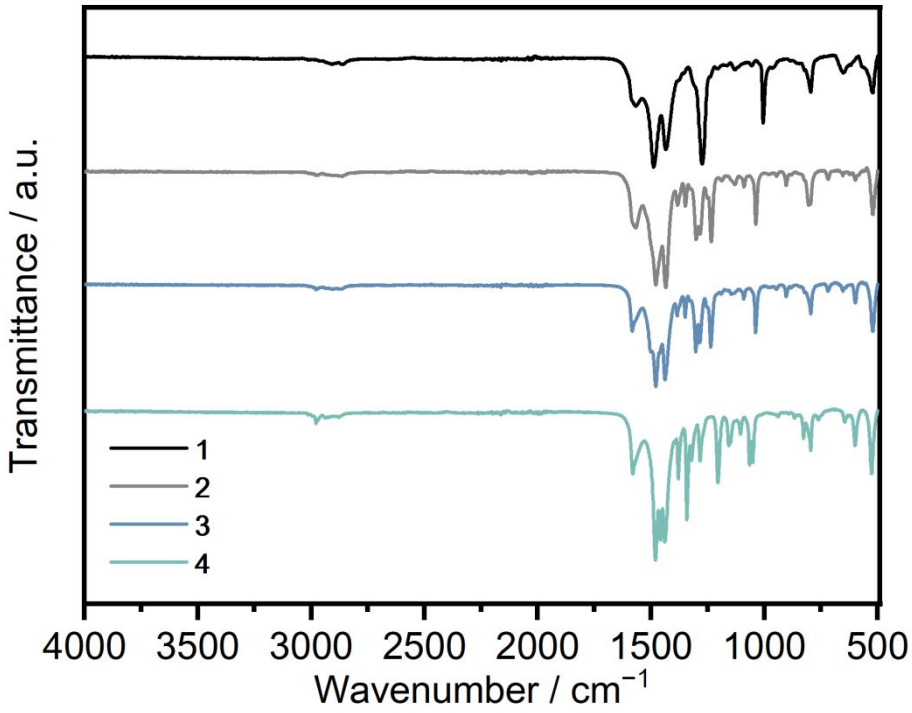

Figure S10. FT-IR spectra of as-synthesized **1**−**4** under Ar.

Table S2. Crystal data and refinement detail for **1**−**4**.

Compound	**1**	**2**	**3**	**4**
Formula	$C_{18}N_6O_{13}Zn_4$	$C_{21}N_6O_{13}Zn_4$	$C_{21}N_6O_{13}Zn_4$	$C_{24}N_6O_{13}Zn_4$
T / K	298			
Wavelength / Å	0.999000			
2θ range / °	2.1−78.2			
Crystal system	Cubic			
Space group	*Fm*-3*m*			
a / Å	24.7739	24.8572	24.8893	24.8597
V / Å^3	15205	15359	15418	15363
Z	8			
Number of reflection	864	877	881	877
R_p	0.0307	0.0328	0.0321	0.0326
R_{wp}	0.0390	0.0436	0.0411	0.0428
S	3.89	5.34	5.39	4.14

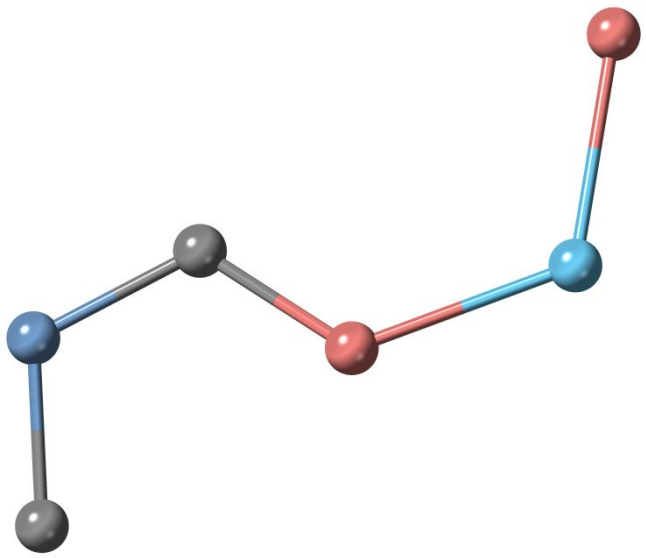

Figure S11. Asymmetric unit of **1**. Zn, O, N, and C atoms are light blue, red, blue, and gray, respectively. The occupancy of the piperazine carbon is 0.5.

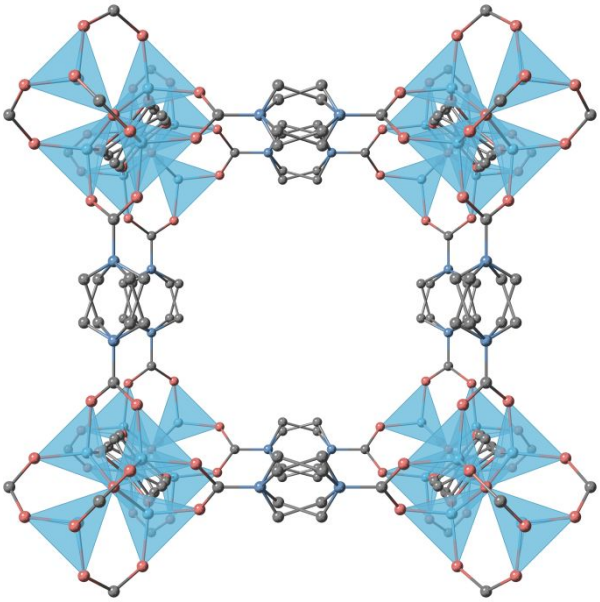

Figure S12. Packing structure of **1**. The PDC linkers show a static disorder.

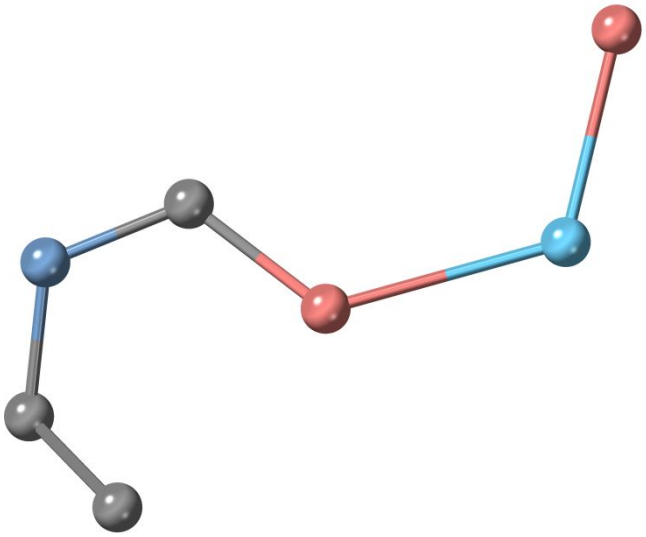

Figure S13. Asymmetric unit of **2**. Zn, O, N, and C atoms are light blue, red, blue, and gray, respectively. The occupancy of the methyl carbon and piperazine carbon are 0.125 and 0.5, respectively.

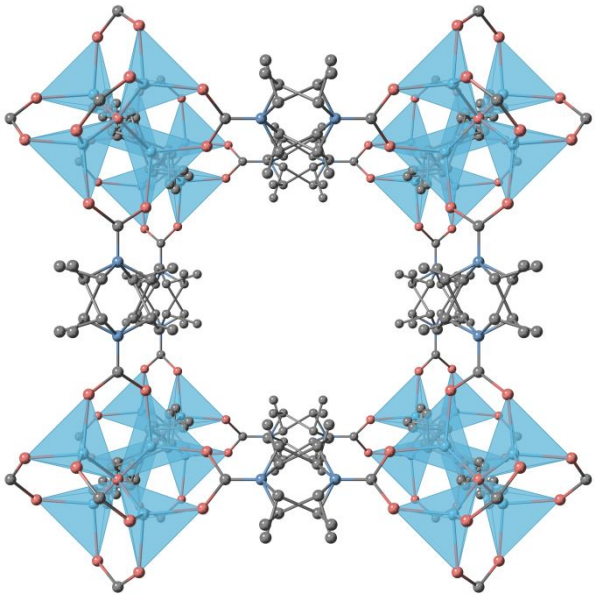

Figure S14. Packing structure of **2**. The *S*-mPDC linkers show a static disorder.

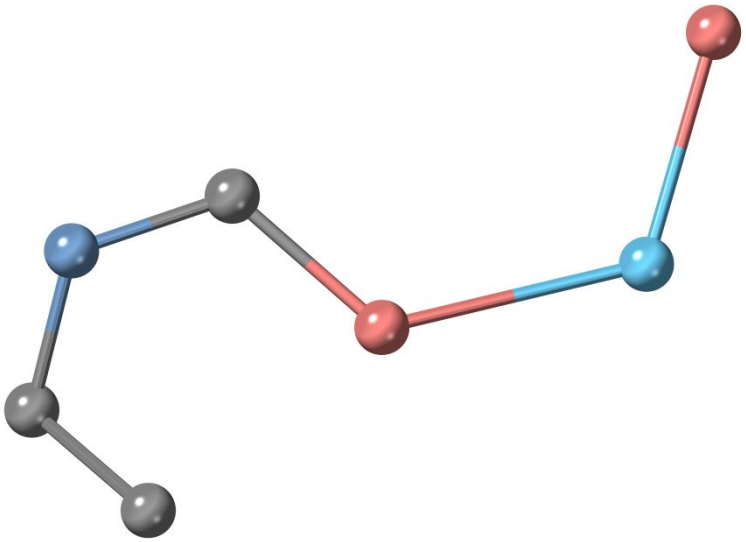

Figure S15. Asymmetric unit of **3**. Zn, O, N, and C atoms are light blue, red, blue, and gray, respectively. The occupancy of the methyl carbon and piperazine carbon are 0.125 and 0.5, respectively.

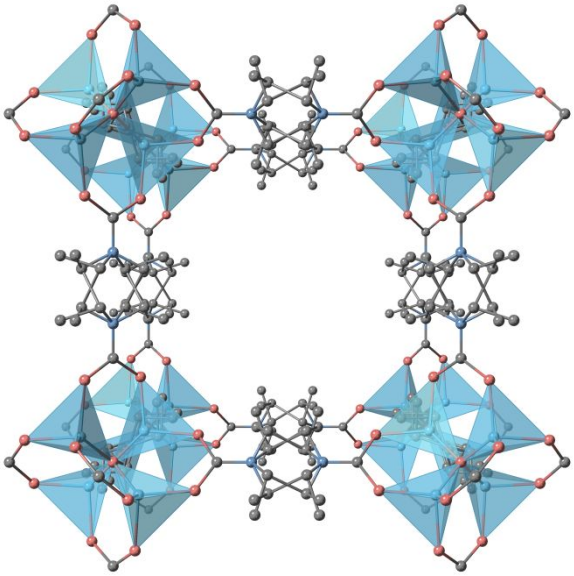

Figure S16. Packing structure of **3**. The *R*-mPDC linkers show a static disorder.

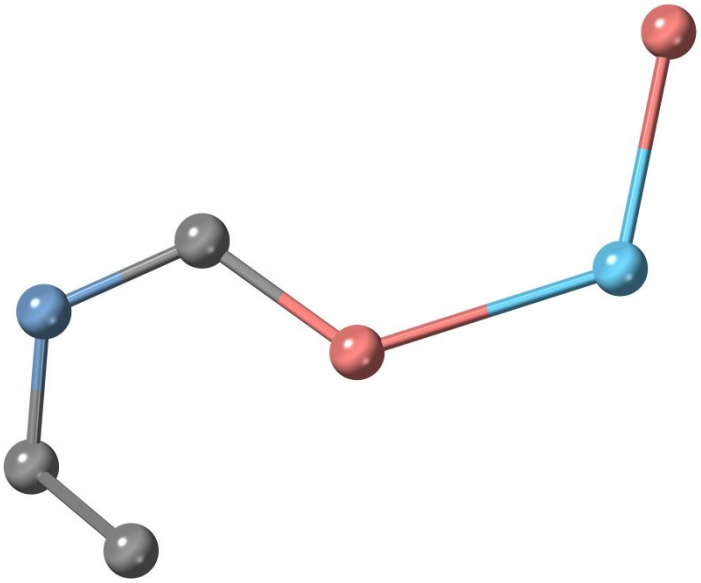

Figure S17. Asymmetric unit of **4**. Zn, O, N, and C atoms are light blue, red, blue, and gray, respectively. The occupancy of the methyl carbon and piperazine carbon are 0.25 and 0.5.

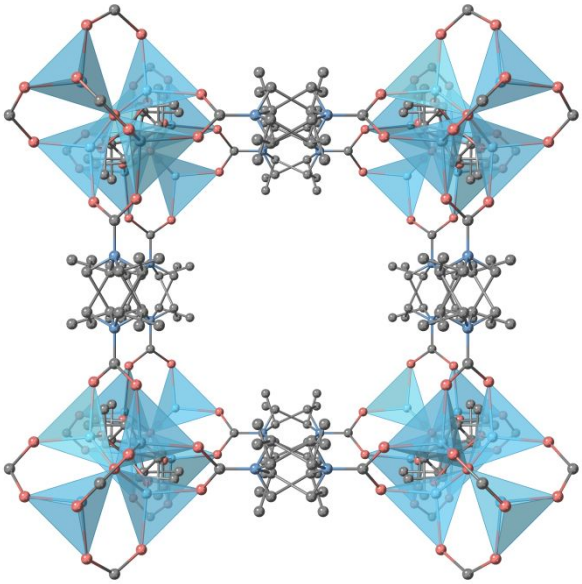

Figure S18. Packing structure of **4**. The dmPDC linkers show a static disorder.

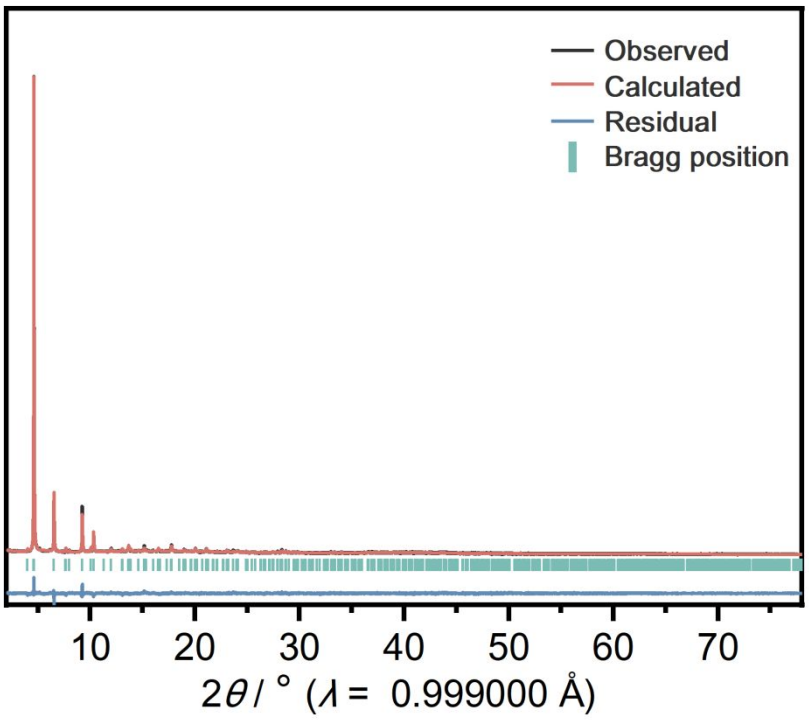

Figure S19. Rietveld refinement of activated **2**.

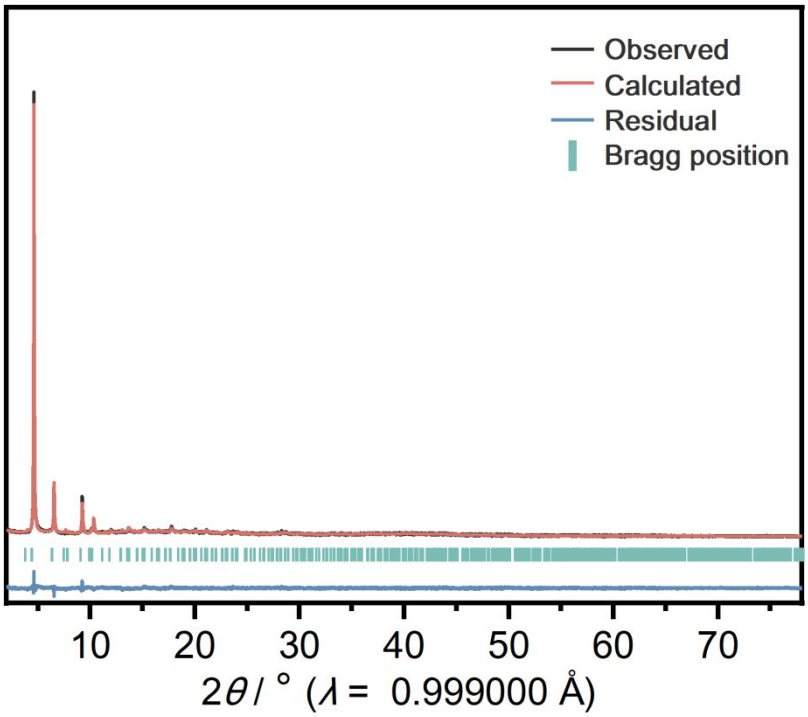

Figure S20. Rietveld refinement of activated **3**.

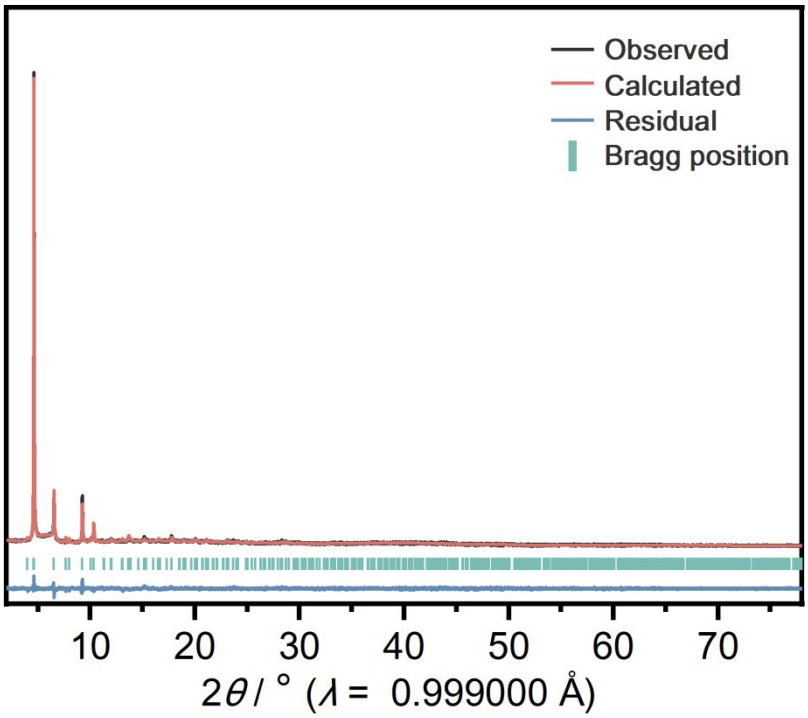

Fig S21. Rietveld refinement of activated **4**.

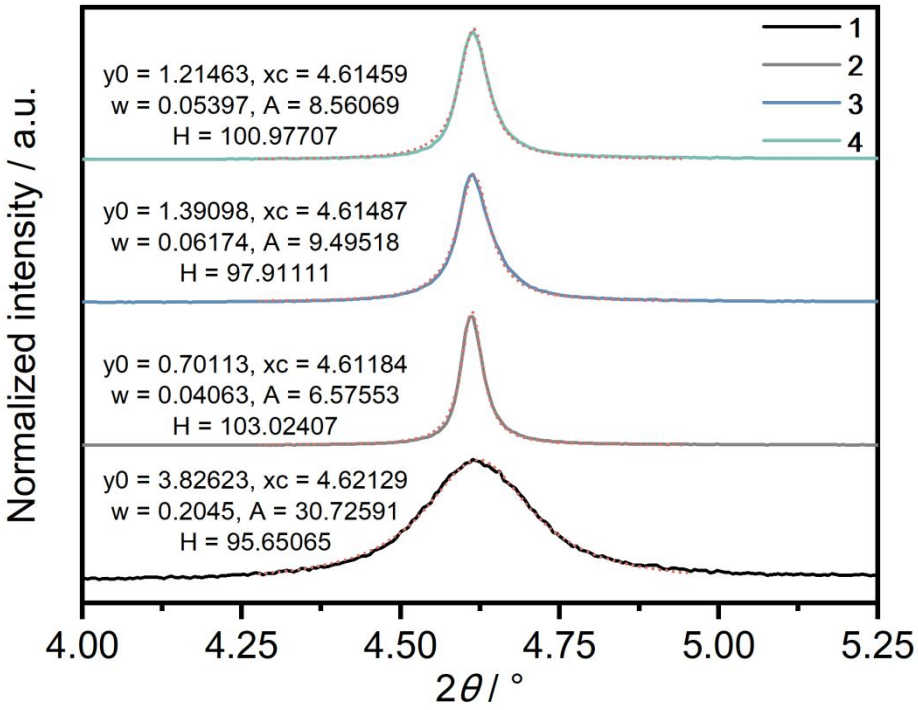

Figure S22. FWHM studies on the first peaks at ca. 4.6° for the activated **1**−**4**.

Table S3. CO_2-derived coordination compounds with porosity.

Compounds	Materials	CO_2-derived species	CO_2 contents / wt%	BET surface areas / $m^2\ g^{-1}$	Ref.
1	MOF/PCP	Carbamate	33.3	1525	This work
2	MOF/PCP	Carbamate	31.6	2366	This work
3	MOF/PCP	Carbamate	31.6	1943	This work
4	MOF/PCP	Carbamate	30.1	1270	This work
$[Zn_3(OCHO)_6]$	MOF/PCP	Formate	56.6	225	9
$[Mg_3(OCHO)_6]$	MOF/PCP	Formate	77.0	504	9
$[Fe_3(OCHO)_6]$	MOF/PCP	Formate	60.7	346	9
$[Co_3(OCHO)_6]$	MOF/PCP	Formate	59.1	324	9
$[Mg_{13}[BH(OCHO)_3]_{12}(BO_3)_4[B(OMe)_3](CH_3CH_2NH)_2]$	MOF/PCP	Formylhydroborate	68.5	356	9
$[Zn_6(CO_3)_4(C_{48}H_{72}N_{12})](CO_3)(NO_3)_2$	MOF/PCP	Carbonate	13.5	8	10
$[Zn_{10}(CO_3)_4(C_9H_6NO)_{12}]$	Discrete complex	Carbonate	6.7	1205	11

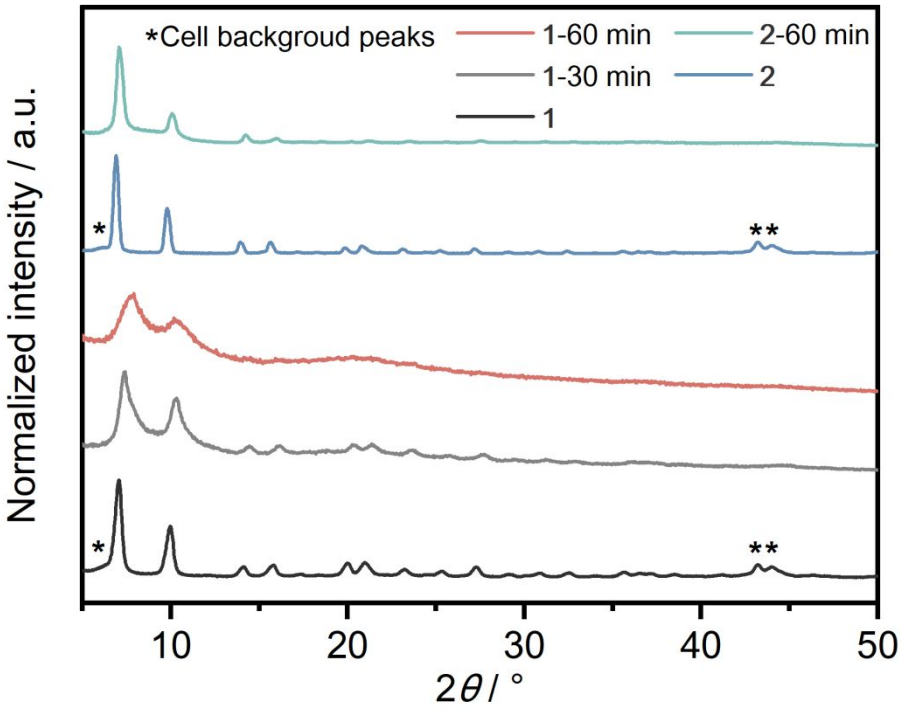

Figure S23. Time-course PXRD patterns of **1** under Ar (black), **1** kept under the air for 30 min (gray) and 60 min (red), **2** under Ar (blue), and **2** kept under the air for 60 min (green).

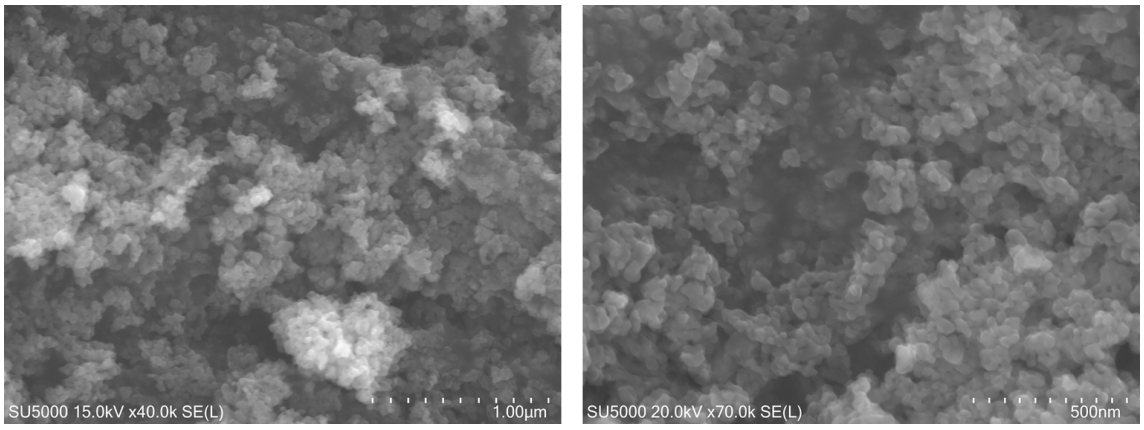

Figure S24. SEM images of activated **1**.

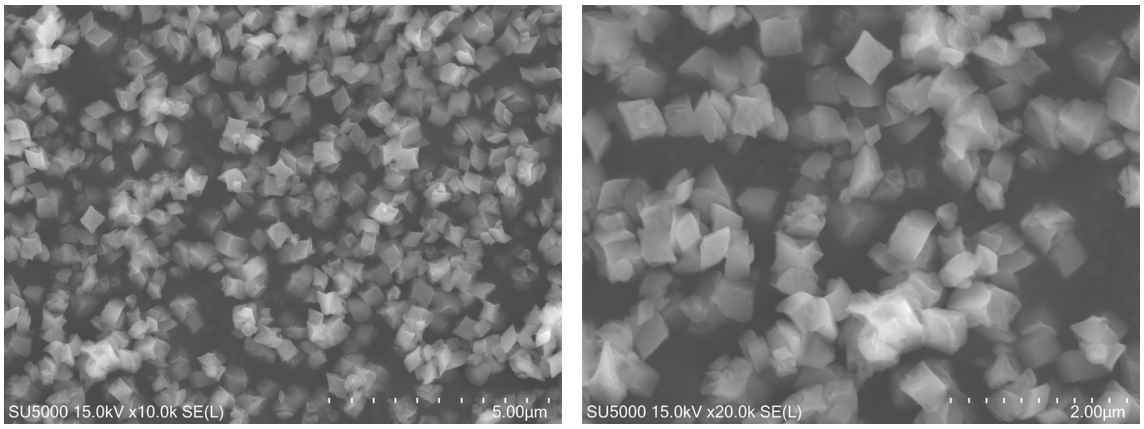

Figure S25. SEM images of activated **2**.

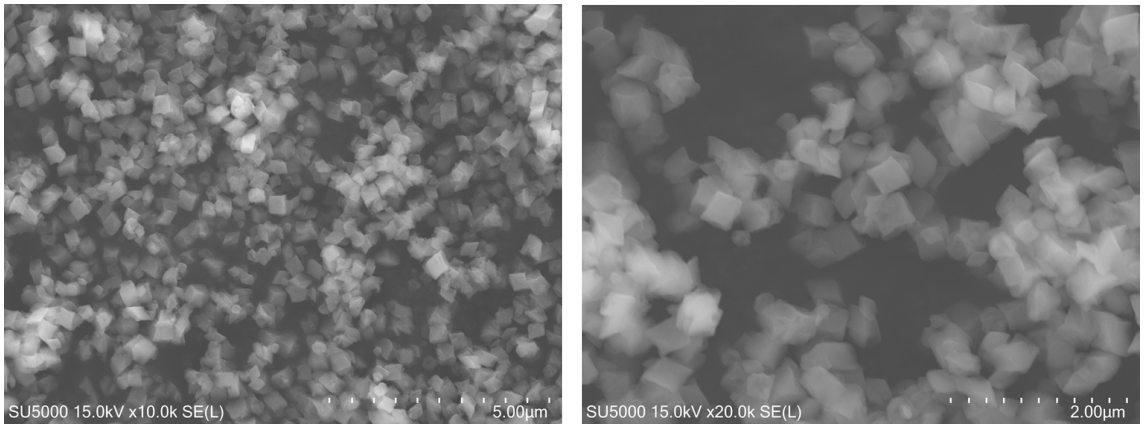

Figure S26. SEM images of activated **3**.

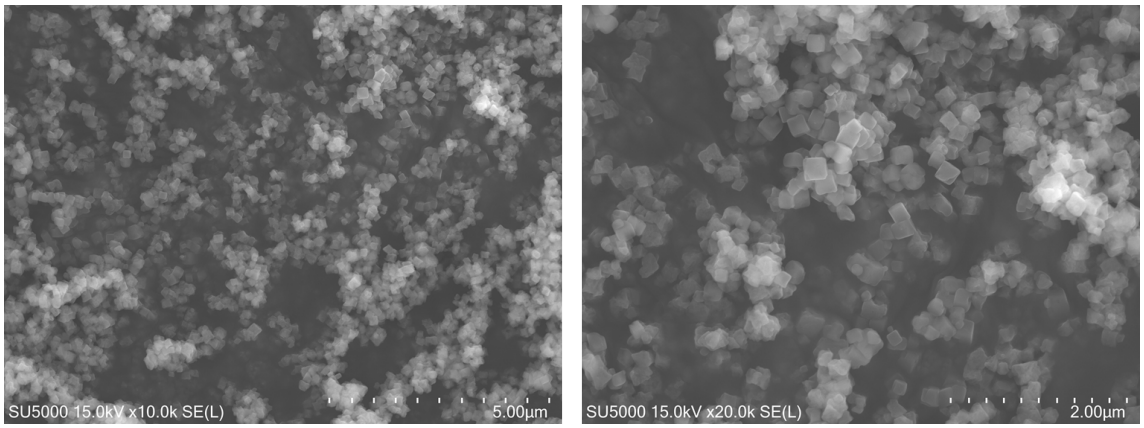

Figure S27. SEM images of activated **4**.

Figure S28. Image of the reaction system for the synthesis of **2-large-scale**.

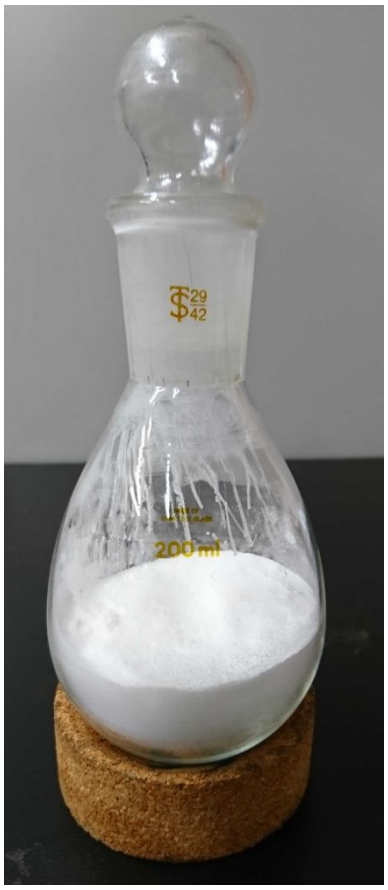

Figure S29. Image of powder sample of **2-large-scale** (ca. 50 g).

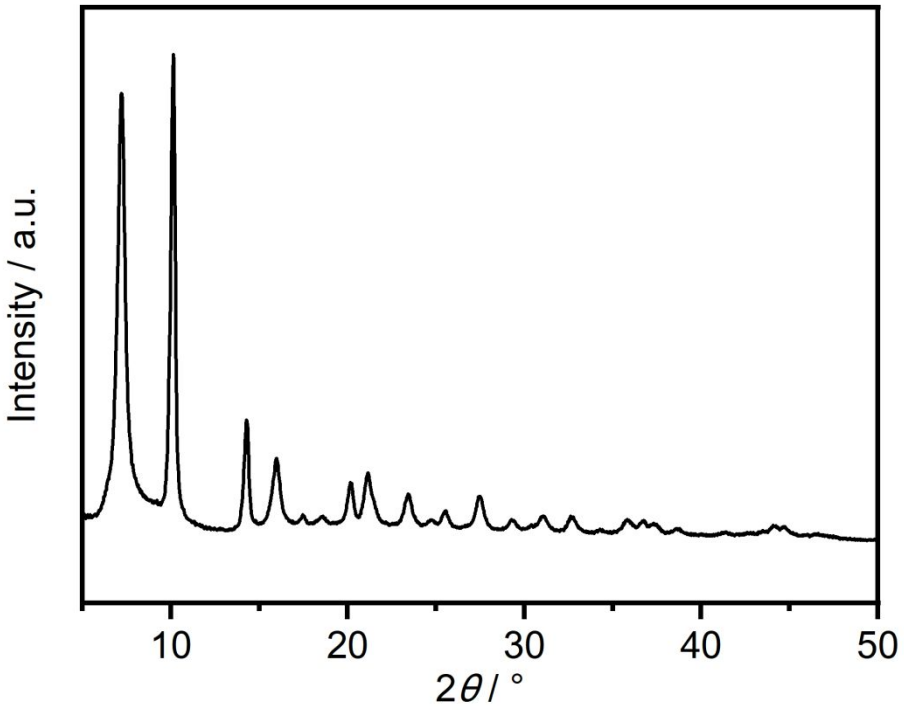

Figure S30. Lab-based PXRD pattern of activated **2-large-scale** under air.

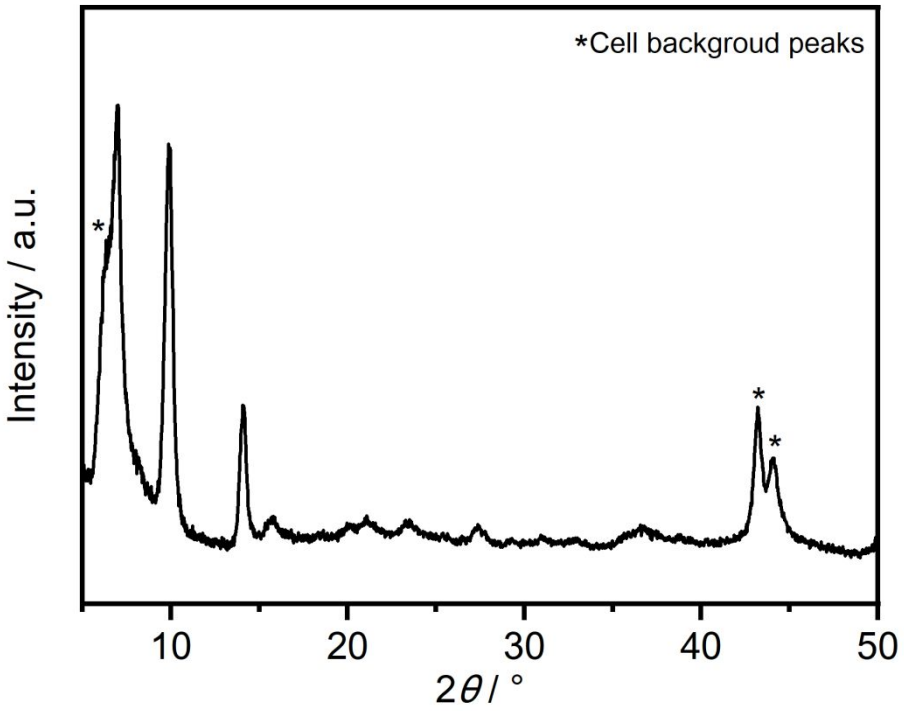

Figure S31. Lab-based PXRD pattern of as-synthesized **1-from-air** under Ar.

Table S4. Gas adsorption properties of the activated **1**−**4**.

	1	**2**	**3**	**4**
N_2 uptake@77 K / mL g^{-1}	486	677	544	394
H_2 uptake@77 K / mL g^{-1}	122	97	153	124
H_2 uptake@87 K / mL g^{-1}	77	67	98	83
CO_2 uptake@195 K / mL g^{-1}	353	187	429	296
CO_2 uptake@298 K / wt%	N.A.	N.A.	37.2 (2.6 MPa)	N.A.
BET surface area / m^2 g^{-1}	1525	2366	1943	1270
Q_{st} for H_2 adsorption / kJ mol^{-1}	6.9	6.3	6.7	7.4

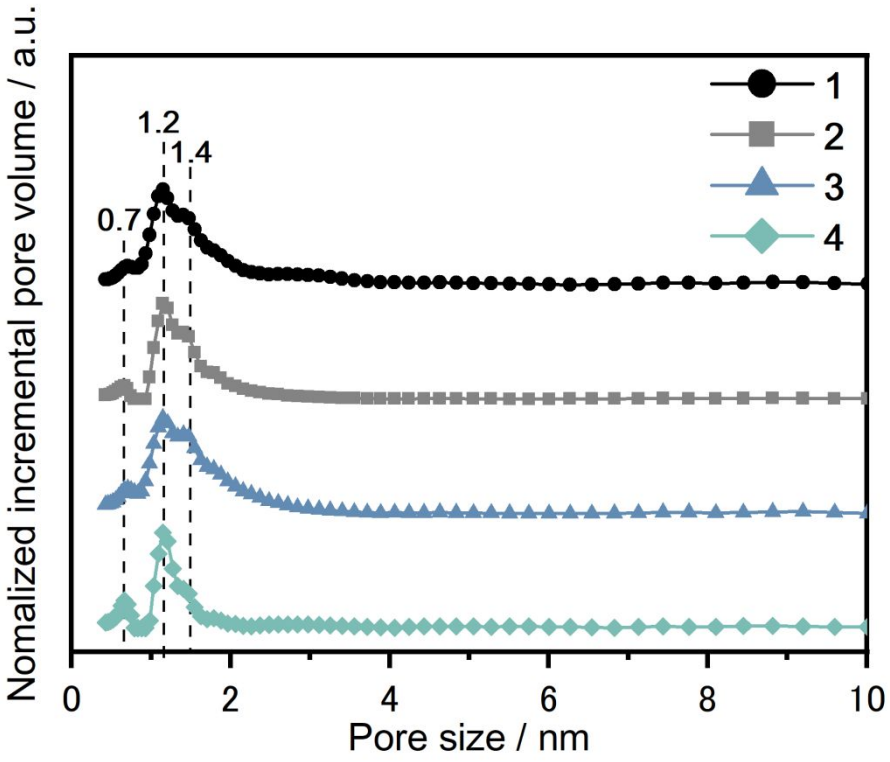

Figure S32. Pore size distributions of **1**−**4** calculated from N_2 adsorption isotherms using the NLDFT method.

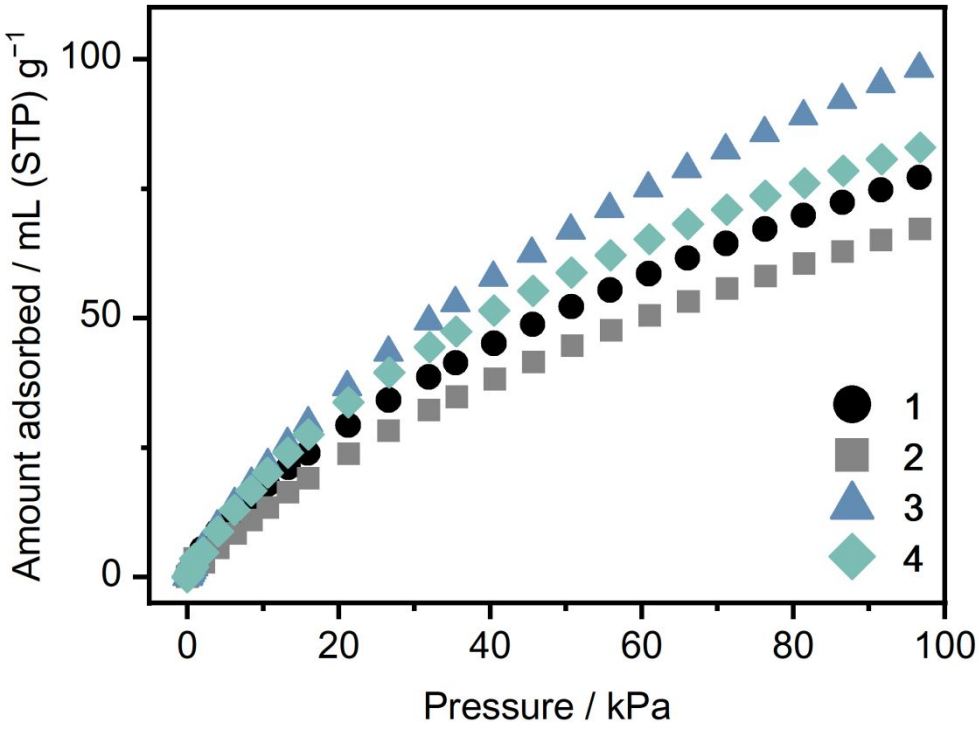

Figure S33. H_2 adsorption isotherms **1**−**4** at 87 K.

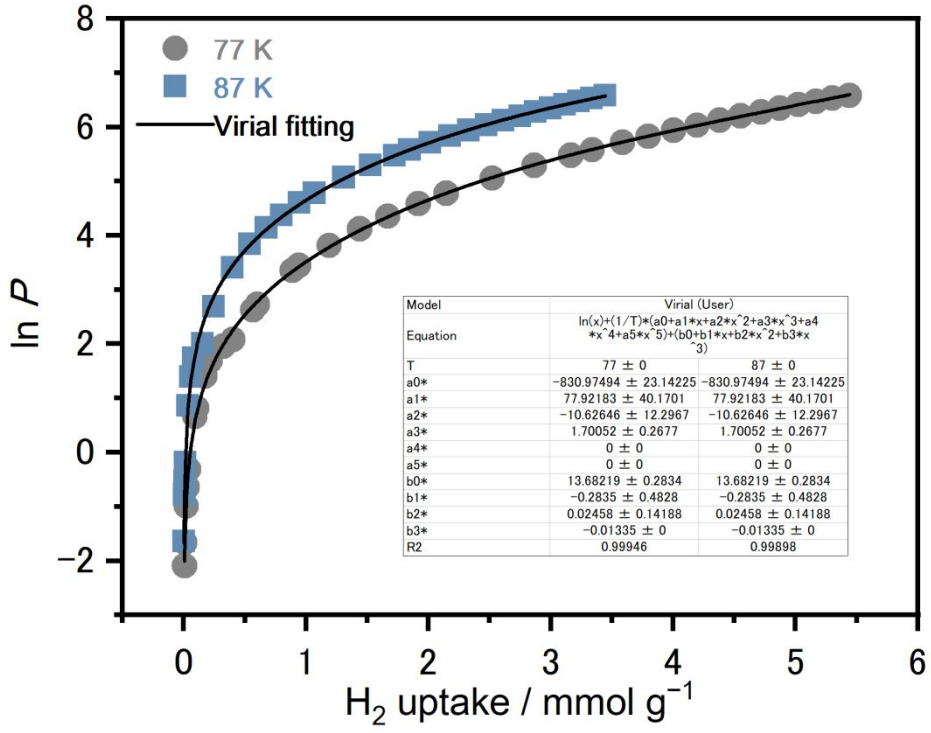

Model	Virial (User)	
Equation	ln(x)+(1/T)*(a0+a1*x+a2*x^2+a3*x^3+a4*x^4+a5*x^5)+(b0+b1*x+b2*x^2+b3*x^3)	
T	77 ± 0	87 ± 0
a0*	−830.97494 ± 23.14225	−830.97494 ± 23.14225
a1*	77.92183 ± 40.1701	77.92183 ± 40.1701
a2*	−10.62646 ± 12.2967	−10.62646 ± 12.2967
a3*	1.70052 ± 0.2677	1.70052 ± 0.2677
a4*	0 ± 0	0 ± 0
a5*	0 ± 0	0 ± 0
b0*	13.68219 ± 0.2834	13.68219 ± 0.2834
b1*	−0.2835 ± 0.4828	−0.2835 ± 0.4828
b2*	0.02458 ± 0.14188	0.02458 ± 0.14188
b3*	−0.01335 ± 0	−0.01335 ± 0
R2	0.99946	0.99898

Figure S34. H_2 adsorption isotherms for **1** at 77 and 87 K, and the respective virial fits.

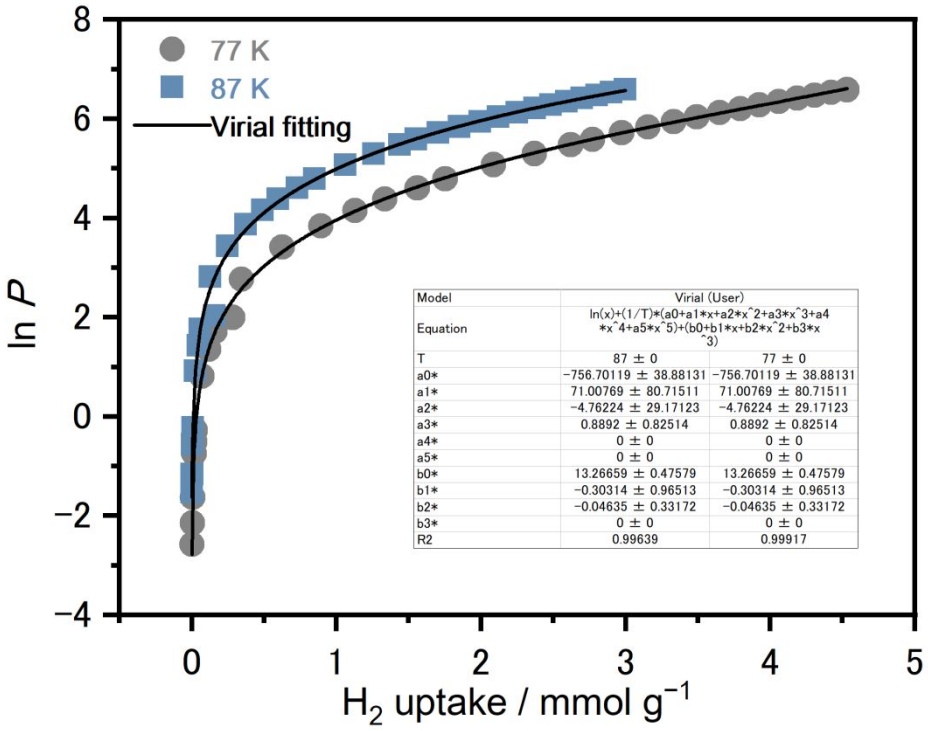

Model	Virial (User)	
Equation	ln(x)+(1/T)*(a0+a1*x+a2*x^2+a3*x^3+a4*x^4+a5*x^5)+(b0+b1*x+b2*x^2+b3*x^3)	
T	87 ± 0	77 ± 0
a0*	−756.70119 ± 38.88131	−756.70119 ± 38.88131
a1*	71.00769 ± 80.71511	71.00769 ± 80.71511
a2*	−4.76224 ± 29.17123	−4.76224 ± 29.17123
a3*	0.8892 ± 0.82514	0.8892 ± 0.82514
a4*	0 ± 0	0 ± 0
a5*	0 ± 0	0 ± 0
b0*	13.26659 ± 0.47579	13.26659 ± 0.47579
b1*	−0.30314 ± 0.96513	−0.30314 ± 0.96513
b2*	−0.04635 ± 0.33172	−0.04635 ± 0.33172
b3*	0 ± 0	0 ± 0
R2	0.99639	0.99917

Figure S35. H_2 adsorption isotherms for **2** at 77 and 87 K, and the respective virial fits.

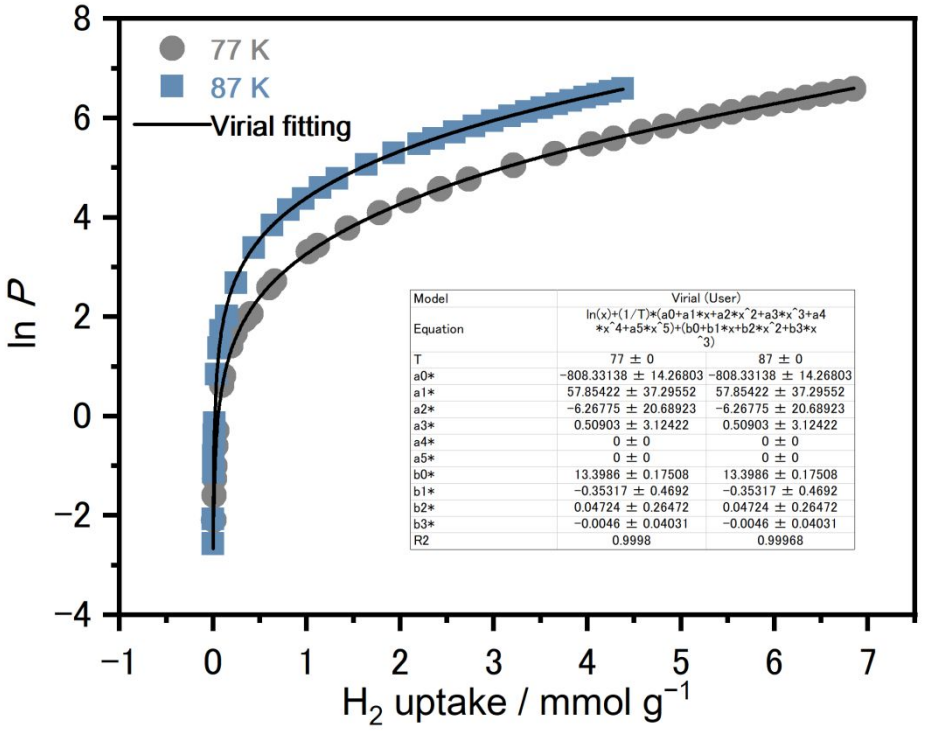

Model	Virial (User)	
Equation	ln(x)+(1/T)*(a0+a1*x+a2*x^2+a3*x^3+a4*x^4+a5*x^5)+(b0+b1*x+b2*x^2+b3*x^3)	
T	77 ± 0	87 ± 0
a0*	−808.33138 ± 14.26803	−808.33138 ± 14.26803
a1*	57.85422 ± 37.29552	57.85422 ± 37.29552
a2*	−6.26775 ± 20.68923	−6.26775 ± 20.68923
a3*	0.50903 ± 3.12422	0.50903 ± 3.12422
a4*	0 ± 0	0 ± 0
a5*	0 ± 0	0 ± 0
b0*	13.3986 ± 0.17508	13.3986 ± 0.17508
b1*	−0.35317 ± 0.4692	−0.35317 ± 0.4692
b2*	0.04724 ± 0.26472	0.04724 ± 0.26472
b3*	−0.0046 ± 0.04031	−0.0046 ± 0.04031
R2	0.9998	0.99968

Figure S36. H_2 adsorption isotherms for **3** at 77 and 87 K, and the respective virial fits.

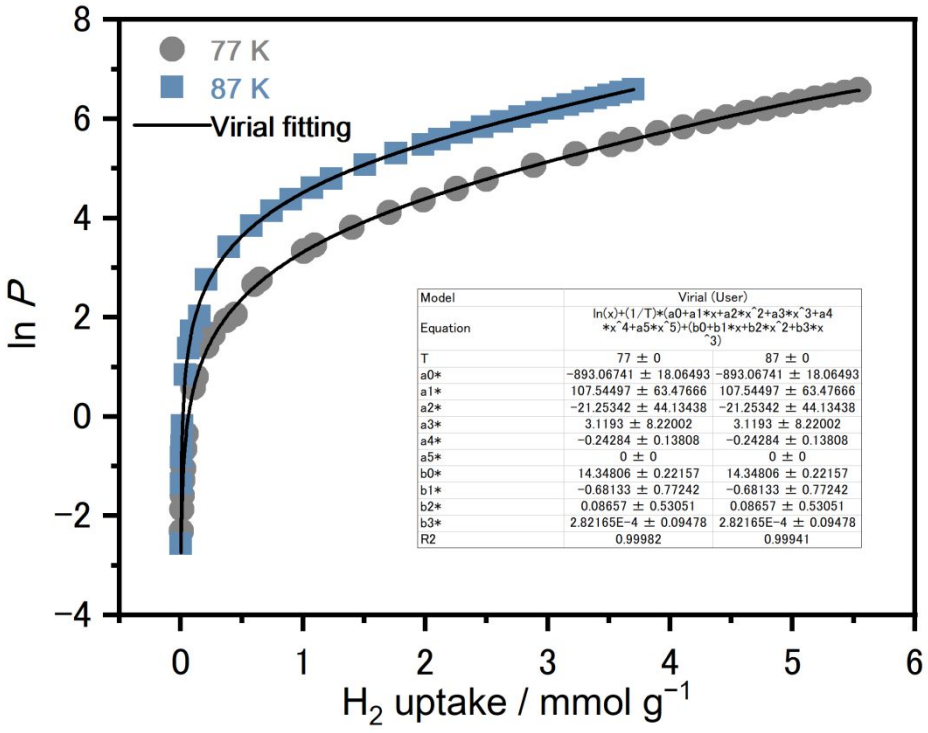

Figure S37. H_2 adsorption isotherms for **4** at 77 and 87 K, and the respective virial fits.

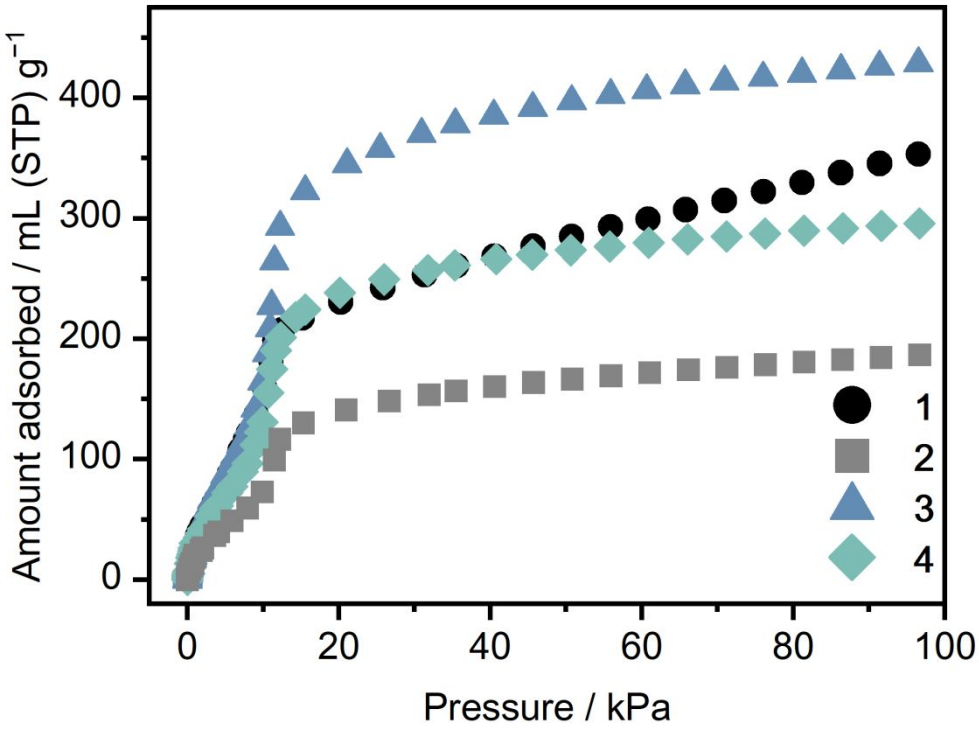

Figure S38. CO_2 adsorption isotherms **1**−**4** at 195 K.

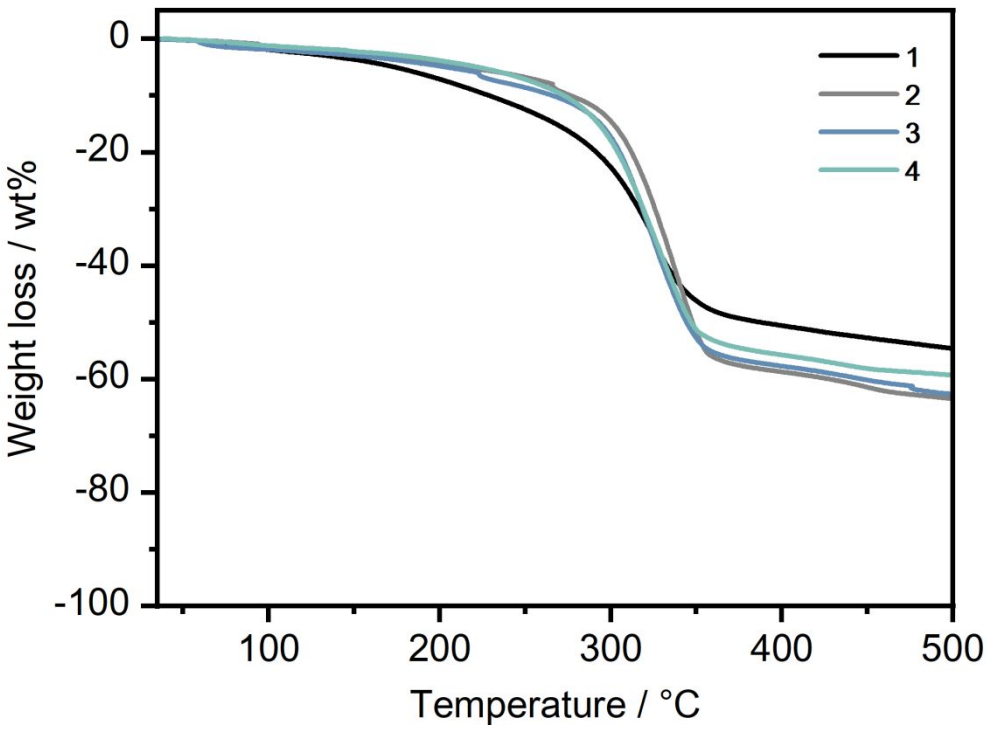

Figure S39. TGA profiles of activated **1**−**4** under Ar.

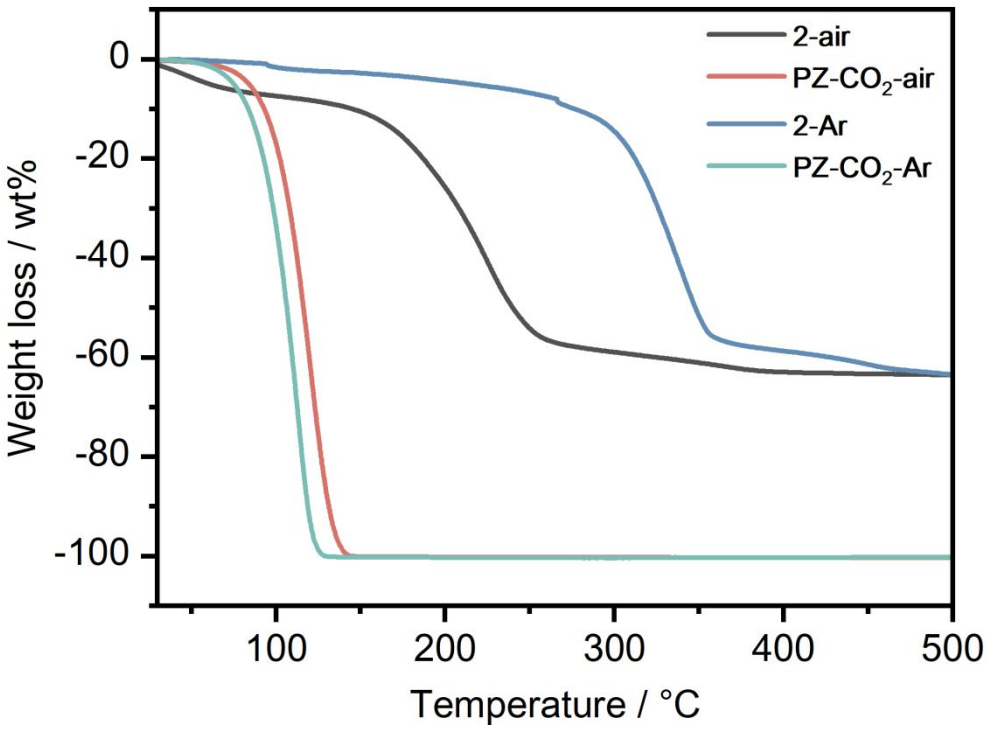

Figure S40. TGA profiles **2** and **PZ-CO_2** under Ar and air.

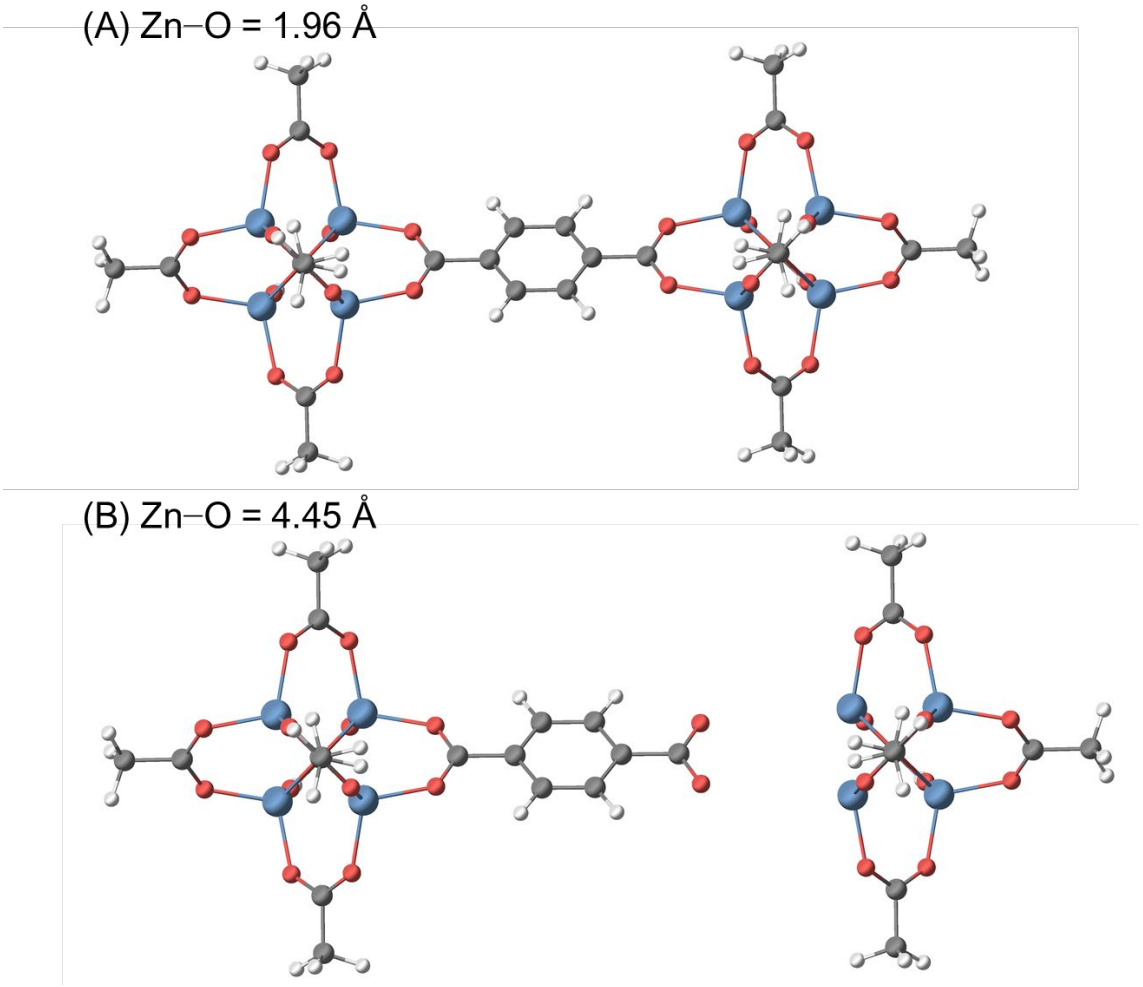

Figure S41. Structures of $[Zn_4O(OAc)_5]_2(BDC)$ calculated by the DFT using a hybrid exchange-correlation functional at the Zn−O distance of (i, top) 1.96 and (ii, bottom) 4.45 Å, respectively. Zn, O, C, and H atoms are blue, red, blue, gray, and white, respectively.

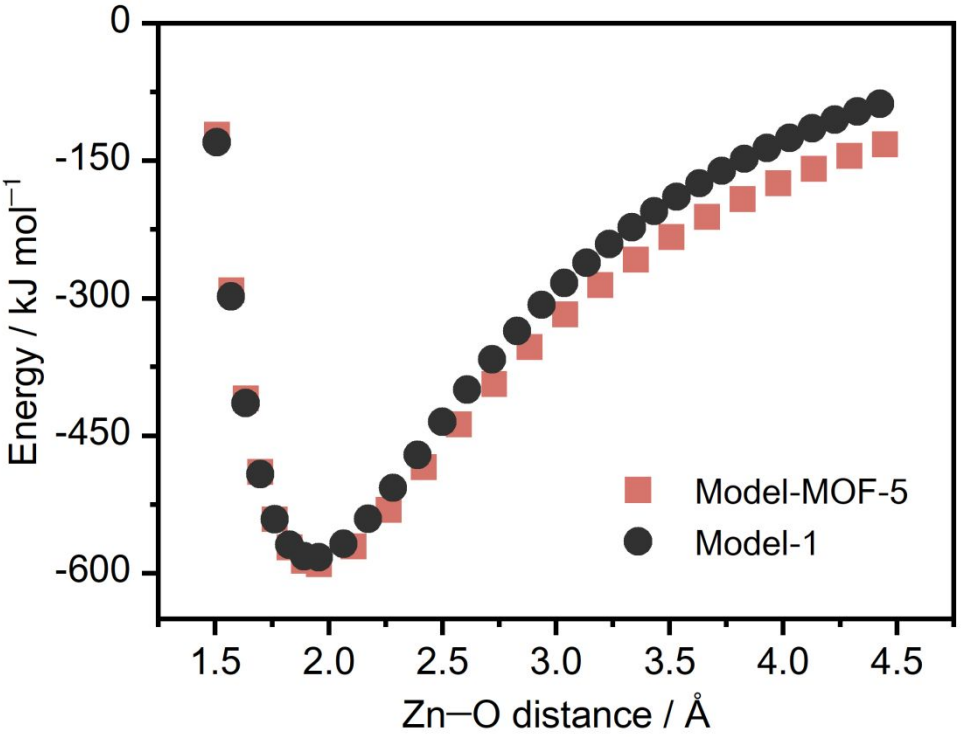

Figure S42. Potential energy curves as a function of Zn−O distance calculated for the models of **1** and MOF-5.

Table S5. Crystal data and refinement detail for **PZ-CO_2** and **PZ-CO_2-DBU**.

Compound	**PZ-CO_2**	**PZ-CO_2-DBU**
Formula	$C_{10}H_{20}N_4O_4$	$C_{28}H_{48}N_8O_4$
MW / g mol^{-1}	260.3	560.7
T / K	103	93
Crystal system	Triclinic	Triclinic
Space group	P-1	$P2_1/c$
Z	1	2
a / Å	5.9351(5)	11.5278(4)
b / Å	6.3960(6)	15.6465(5)
c / Å	9.0648(8)	8.4678(3)
α / °	94.258(7)	90
β / °	106.223(7)	104.363(3)
γ / °	113.697(8)	90
V / Å^3	295.66(5)	1479.60(9)
μ / mm^{-1}	0.114	0.086
Reflections collected	4009	13593
Independent reflections	1433	3815
R ($I > 2.00\sigma(I)$, all data)	0.0468, 0.0404	0.0466, 0.0379
R_w ($I > 2.00\sigma(I)$, all data)	0.1119, 0.1069	0.0979, 0.0939
GOF on F^2	1.065	1.023

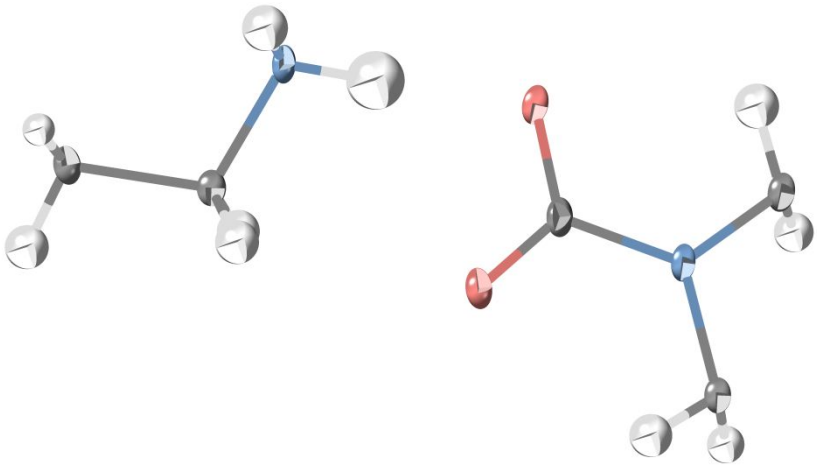

Figure S43. ORTEP diagram of the asymmetric unit of **PZ-CO_2**. O, N, C, and H atoms are red, blue, gray, and white, respectively.

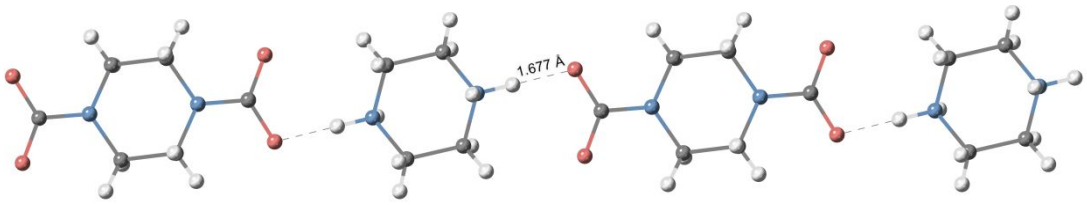

Figure S44. One-dimensional hydrogen bonding network between H_4PZ^{2+} and $[PZ(CO_2)_2]^{2-}$ in **PZ-CO$_2$**. O, N, C, and H atoms are red, blue, gray and white, respectively.

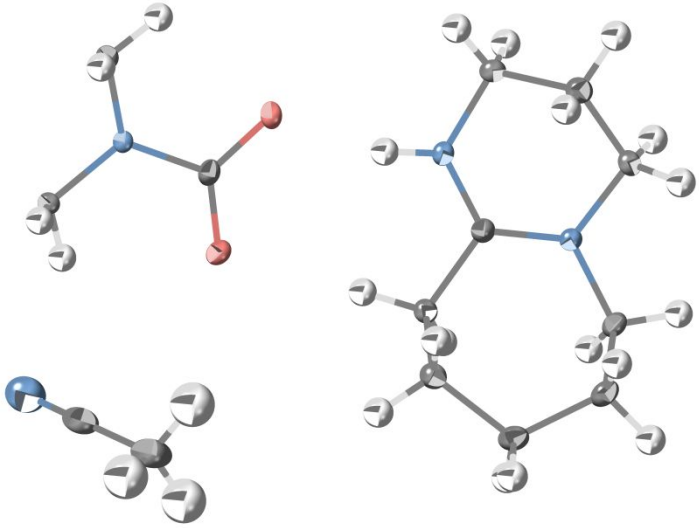

Figure S45. ORTEP diagram of the asymmetric unit of **PZ-CO$_2$-DBU**. O, N, C, and H atoms are red, blue, gray, and white, respectively.

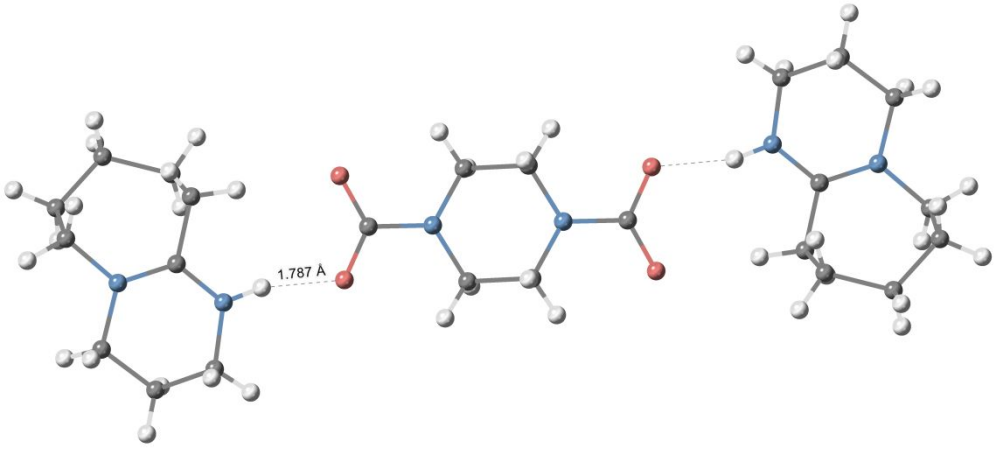

Figure S46. Hydrogen bonding between $HDBU^+$ and $[PZ(CO_2)_2]^{2-}$ in **PZ-CO$_2$**. O, N, C, and H atoms are red, blue, gray, and white, respectively.

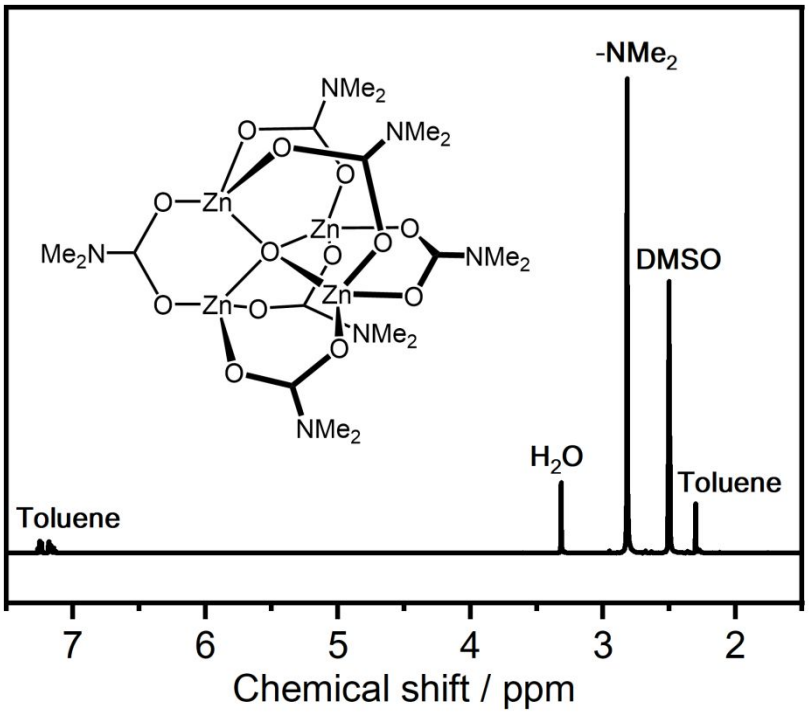

Figure S47. ^{1}H NMR of **Zn-SBU** dissolved in DMSO-d_6.

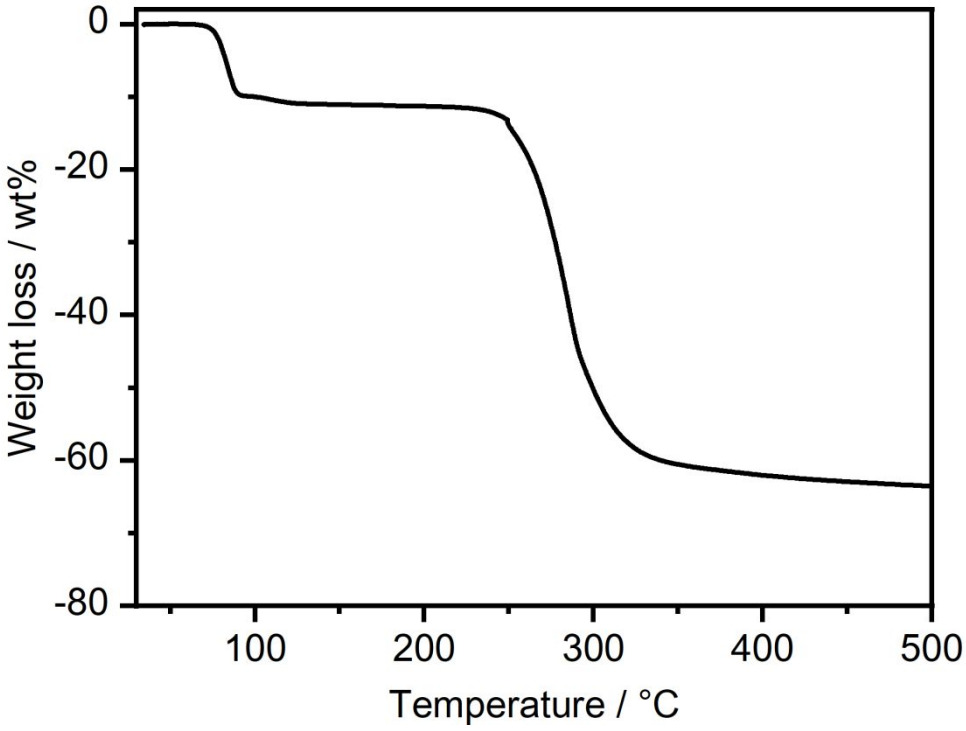

Figure S48. TGA profile of **Zn-SBU** under Ar.

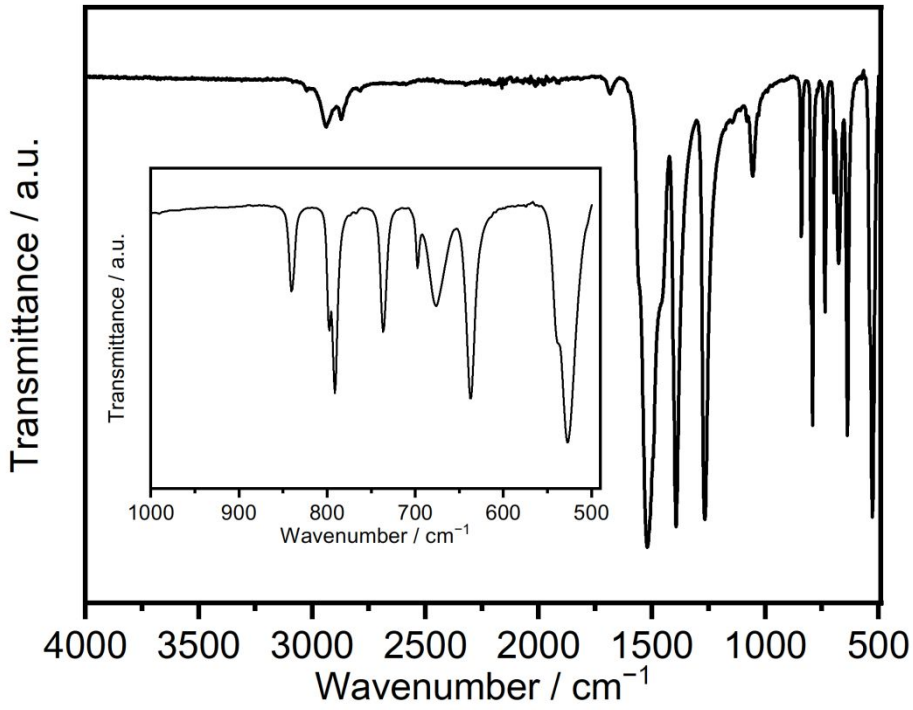

Figure S49. IR spectrum of **Zn-SBU** under Ar.

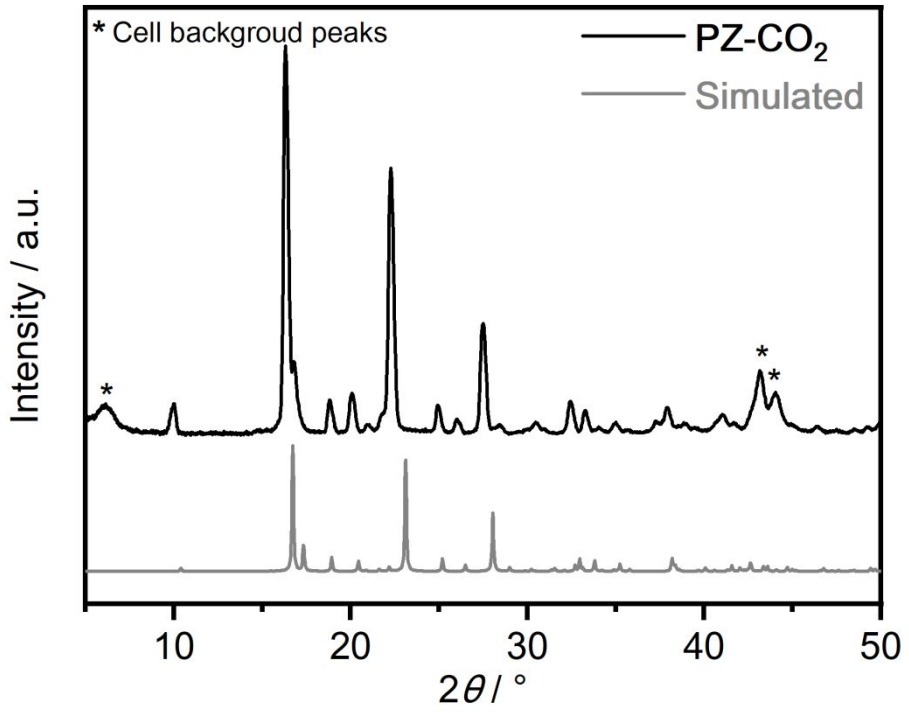

Figure S50. PXRD patterns of experimental and simulated **PZ-CO$_2$** under Ar.

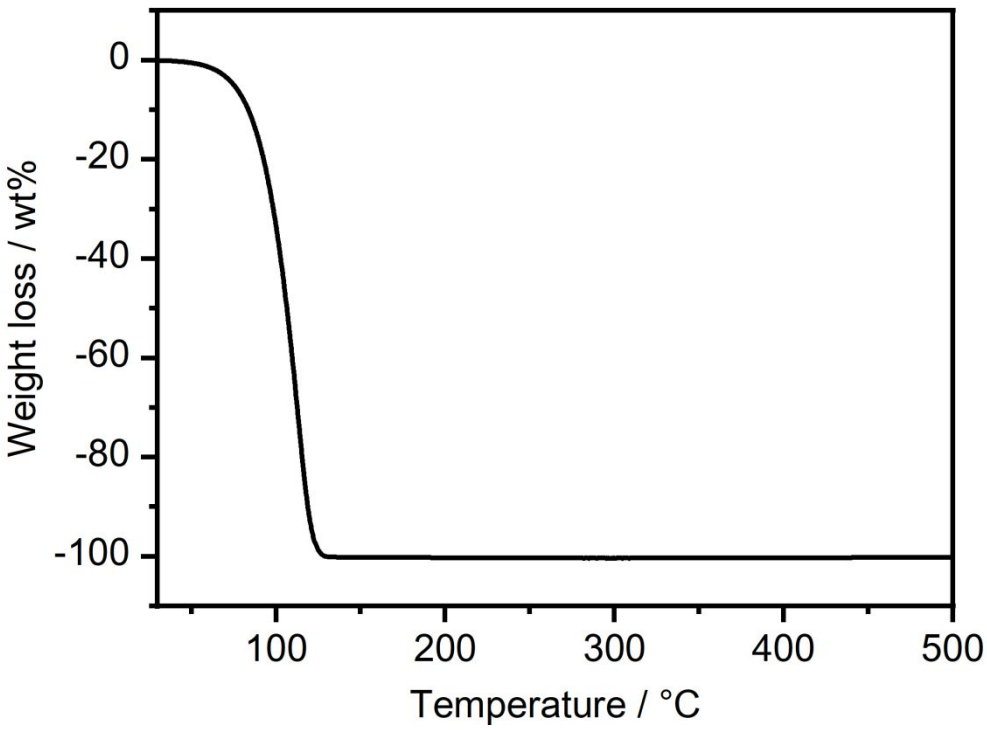

Figure S51. TGA profile of **PZ-CO_2** under Ar.

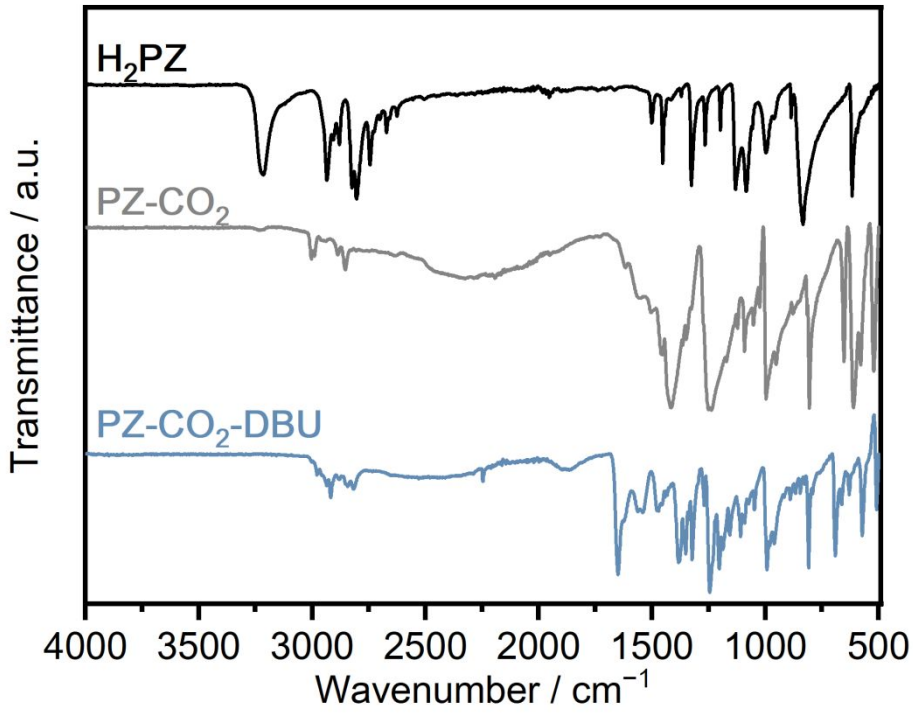

Figure S52. IR spectra of **H_2PZ**, P**Z-CO_2**, and **PZ-CO_2-DBU** under Ar.

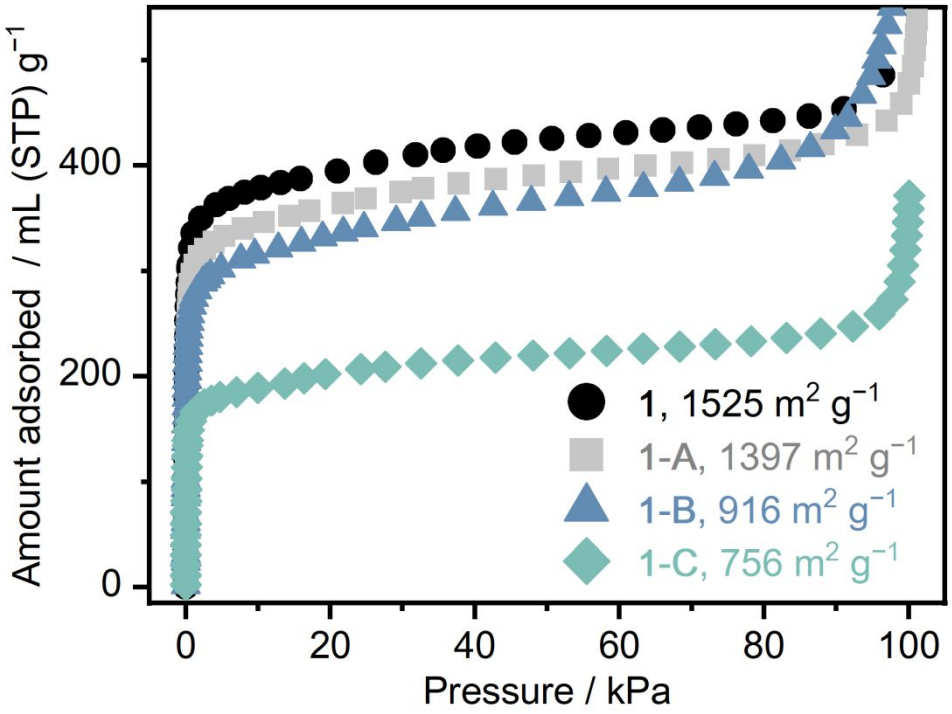

Figure S53. N_2 adsorption isotherms of **1**, **1-A**, **1-B**, and **1-C** at 77 K.

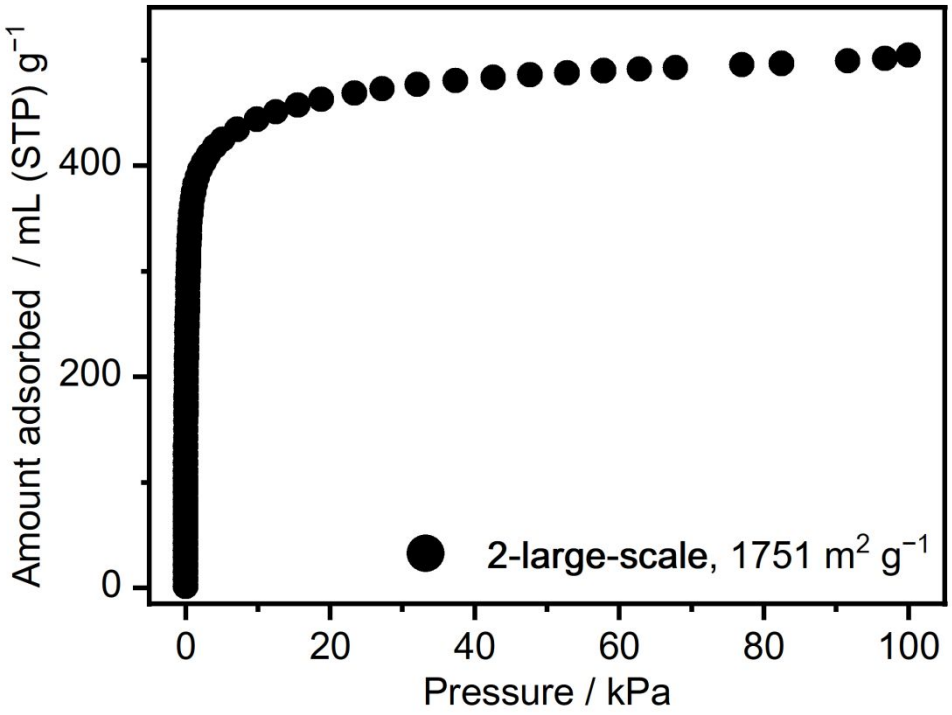

Figure S54. N_2 adsorption isotherm of **2-large-scale** at 77 K.

References

(1) Blum, V.; Gehrke, R.; Hanke, F.; Havu, P.; Havu, V.; Ren, X.; Reuter, K.; Scheffler, M., Ab initio molecular simulations with numeric atom-centered orbitals. *Comput. Phys. Commun.* **2009,** *180* (11), 2175-2196.

(2) Perdew, J. P.; Burke, K.; Ernzerhof, M., Generalized Gradient Approximation Made Simple. *Phys. Rev. Lett.* **1996,** *77* (18), 3865-3868.

(3) Tkatchenko, A.; Scheffler, M., Accurate Molecular Van Der Waals Interactions from Ground-State Electron Density and Free-Atom Reference Data. *Phys. Rev. Lett.* **2009,** *102* (7), 073005.

(4) Janesko, B. G.; Henderson, T. M.; Scuseria, G. E., Screened hybrid density functionals for solid-state chemistry and physics. *Phys. Chem. Chem. Phys.* **2009,** *11* (3), 443-454.

(5) Perdew, J. P.; Wang, Y., Accurate and simple analytic representation of the electron-gas correlation energy. *Phys. Rev. B* **1992,** *45* (23), 13244-13249.

(6) Dell'Amico, D. B.; Calderazzo, F.; Labella, L.; Marchetti, F., A facile synthesis of $Zn_4(\mu_4\text{-}O)(O_2CNMe_2)_6$. *Inorg. Chem. Acta* **2003,** *350*, 661-664.

(7) Dell'Amico, D. B.; Calderazzo, F.; Labella, L.; Marchetti, F.; Mazzoncini, I., *N,N*-dimethylcarbamato complexes of zinc. *Inorg. Chem. Acta* **2006,** *359* (10), 3371-3374.

(8) Sim, J.; Jo, E.; Jhon, Y. H.; Jang, S. G.; Shim, J.-G.; Jang, K.-R.; Paek, K.; Kim, J., Isolation and Crystal Structure Determination of Piperazine Dicarbamate Obtained from a Direct Reaction between Piperazine and Carbon Dioxide in Methanol. *Bull. Korean Chem. Soc.* **2016,** *37* (11), 1854-1857.

(9) Kadota, K.; Duong, N. T.; Nishiyama, Y.; Sivaniah, E.; Horike, S., Synthesis of porous coordination polymers using carbon dioxide as a direct source. *Chem. Commun.* **2019,** *55* (63), 9283-9286.

(10) Swamy, S. I.; Bacsa, J.; Jones, J. T. A.; Stylianou, K. C.; Steiner, A.; Ritchie, L. K.; Hasell, T.; Gould, J. A.; Laybourn, A.; Khimyak, Y. Z.; Adams, D. J.; Rosseinsky, M. J.; Cooper, A. I., A Metal–Organic Framework with a Covalently Prefabricated Porous Organic Linker. *J. Am. Chem. Soc.* **2010,** *132* (37), 12773-12775.

(11) Sokołowski, K.; Bury, W.; Justyniak, I.; Fairen-Jimenez, D.; Sołtys, K.; Prochowicz, D.; Yang, S.; Schröder, M.; Lewiński, J., Permanent Porosity Derived From the Self-Assembly of Highly Luminescent Molecular Zinc Carbonate Nanoclusters. *Angew. Chem. Int. Ed.* **2013,** *52* (50), 13414-13418.